International Journal of Bifurcation and Chaos, Vol. 30, No. 7 (2020) 2050110 (32 pages)

DOI: 10.1142/S0218127420501102

Input–Output Characterization of the Dynamical Properties of Circuits with a Memelement

Giacomo Innocenti[*,‡], Mauro Di Marco[†,§], Alberto Tesi[*,¶] and Mauro Forti[†,‖]

[*]*Department of Information Engineering, University of Florence, via S. Marta 3 – 50139 Firenze, Italy*

[†]*Department of Information Engineering and Mathematics, University of Siena, via Roma 56 – 53100 Siena, Italy*

[‡]*giacomo.innocenti@unifi.it*

[§]*dimarco@diism.unisi.it*

[¶]*alberto.tesi@unifi.it*

[‖]*forti@diism.unisi.it*

Received December 5, 2019

The paper proposes a novel input–output approach to characterize the dynamical properties of a class of circuits composed by a linear time-invariant two-terminal element coupled with one of the ideal memelements (memory elements) introduced by Prof. L. O. Chua, i.e. memristors, memcapacitors, and meminductors. The developed approach permits to readily determine the conditions under which the dynamics of any circuit of the class admits a first integral. It is also shown that the circuit dynamics can be obtained by collecting the dynamical behaviors displayed by a canonical reduced-order input–output system subject to a constant input of any amplitude. Notably, the reduced-order system exactly describes the dynamics of a circuit forced by a constant generator and with a nonlinear memoryless element in place of the memelement. The relation between the proposed input–output approach and the available state space ones (e.g. Flux-Charge Analysis Method (FCAM)) is also addressed. The main result is that explicit expressions of the invariant manifolds can be directly obtained in the voltage–current state space. Finally, it is shown how the approach also applies to circuits which contain forcing generators. It is believed that the proposed input–output approach can be a useful alternative to state space methods for studying multistability and control issues.

Keywords: Memristive circuits; input–output representation; nonlinear dynamics; invariant manifolds; multistability.

1. Introduction

The first electronic implementation at Hewlett and Packard of memristor (memory resistor) in 2008 [Strukov *et al.*, 2008] generated a strong renewed worldwide interest in the fourth fundamental circuit element introduced in 1971 by Prof. L. O. Chua [Chua, 1971]. More recently, an increasing interest has been devoted also to memcapacitors and meminductors, the elements proposed to model memory effects for capacitors and inductors [Di Ventra *et al.*,

[¶]Author for correspondence

This work was supported by MUR (Ministero dell'Universitáe della Ricerca) under Grant 2017LSCR4K_003.

2009]. This is witnessed by the number of contributions concerning physical modeling, theoretic analysis, simulations, implementation and applications of memcapacitors and meminductors [Pershin & Di Ventra, 2011; Radwan & Fouda, 2015; Pei *et al.*, 2015; Biolek *et al.*, 2011; Li *et al.*, 2013; Biolek *et al.*, 2013; Georgiou *et al.*, 2018].

Memristors, memcapacitors and meminductors, which are also termed memelements, have rapidly gained a prominent role as completely new electrical components with unconventional functions and dynamics that are capable of outperforming similar CMOS implementations to sustain the growth of the electronics industry at the end of Moore's law [Waldrop, 2016; Williams, 2017; Zidan *et al.*, 2018]. On-chip memory, biologically inspired computing and in-memory computing, i.e. the integration of storage and computation in the same physical location [Li *et al.*, 2019], are categories that are expected to significantly benefit from memelement developments. This is in turn particularly relevant to future computing needs as cognitive processing, big-data analysis and low-power intelligent systems based on the Internet of Things. A new era for computational systems can be foreseen based on new analogue and non-Boolean computational schemes for real time processing owing to the possibility of attaining via the use of memelements high bandwidths with much reduced power consumption [Mazumder *et al.*, 2012; Tetzlaff, 2014; Adamatzky & Chua, 2014; Traversa & Di Ventra, 2015; Chua, 2015; Pérez-Tomás, 2019].

This huge interest towards the use of memelements in several applications has motivated the need to deeply understand the dynamical properties of circuits containing these memory elements. Indeed, it has been well established that the state space of circuits containing ideal memristors is "foliated", i.e. it can be decomposed in a continuum of invariant manifolds where the circuit dynamics is described by a reduced order system. Specifically, in [Amador *et al.*, 2017; Ponce *et al.*, 2017] it is shown that the dynamics of a third order memristor circuit admits a first integral in the current–voltage domain and hence it can be equivalently described by a family of second order systems indexed by an additional constant parameter. Notably, the existence of a first integral implies that the second order systems have a smoother vector field, which is a useful property when the memristor has a piecewise linear characteristic. In [Corinto & Forti, 2016, 2017] a more systematic technique has been proposed to investigate circuits containing ideal flux- or charge-controlled memristors. The technique, which is referred to as the flux-charge analysis method (FCAM), provides an equivalent state space description of memristor circuits in the flux-charge domain, which is indeed shown to be a more natural domain than the voltage–current one for a deeper understanding of the circuit dynamics. In both cases, the dynamics of the original memristor circuits can be equivalently described by a family of state space reduced-order systems indexed by some constant parameters (usually, one for each memristor), whose values depend on the initial conditions of the memristor circuit and uniquely identify the specific invariant manifold. Hence, changing this parameter (i.e. the initial conditions) implies changing the invariant manifold where the memristor circuit can display either convergent, or oscillatory, or even more complex behaviors. This dynamical richness of ideal memristor circuits is often referred to as "extreme multistability" [Li *et al.*, 2014; Scarabello & Messias, 2014; Messias *et al.*, 2010; Bao *et al.*, 2016; Yuan *et al.*, 2016b; Chang *et al.*, 2019] and involves the so-called "bifurcations without parameters" phenomenon, i.e. bifurcations which are induced without varying the system parameters [Fiedler *et al.*, 2000; Corinto & Forti, 2017]. More recently, FCAM has been extended to much broader classes of circuits containing more than one memristor [Corinto & Forti, 2018; Chen *et al.*, 2020] as well as memcapacitors and meminductors [Corinto *et al.*, 2019; Rajagopal *et al.*, 2018; Yuan *et al.*, 2016a; Yuan *et al.*, 2016b]. Also in this case, it is shown that the original circuit can be equivalently described by a family of state space reduced-order systems indexed by a number of constant parameters, usually equal to the number of ideal memelements.

Several contributions make it clear that circuits containing memelements are able to display a rich variety of multistability phenomena [Li *et al.*, 2014; Scarabello & Messias, 2014; Messias *et al.*, 2010; Bao *et al.*, 2016; Yuan *et al.*, 2016a; Yuan *et al.*, 2016b; Xu *et al.*, 2017; Rajagopal *et al.*, 2018; Varshney *et al.*, 2018; Corinto *et al.*, 2019; Yuan *et al.*, 2019; Wang *et al.*, 2019; Chang *et al.*, 2019; Chen *et al.*, 2020; Zhang *et al.*, 2019]. To this respect, it is worth noting that multistability control is a field of general growing interest (see, e.g. [Pisarchik & Feudel, 2014] and references therein),

also for its connection to the development of new computational paradigms, such as reservoir computing [Appeltant *et al.*, 2011; Jensen & Tufte, 2017]. Indeed, some multistability control aspects have been recently considered for targeting the memristor circuit state space towards the attractors contained in one of the invariant manifolds [Chen *et al.*, 2018; Corinto & Forti, 2018; Di Marco *et al.*, 2019] as well as to mimicking neuron dynamics via a Murali–Lakshmanan–Chua memristor circuit [Innocenti *et al.*, 2019a].

In this paper, an input–output approach is developed for a systematic analysis of the dynamics of classes of circuits containing ideal memelements. Besides being the natural counterpart of state space methods, input–output approaches allow for a thorough use of the several frequency domain tools available for analysis and control purposes. Some preliminary results in this direction have been already obtained in [Di Marco *et al.*, 2018; Innocenti *et al.*, 2019b] for the prediction of limit cycles and their bifurcation in both forced and unforced circuits containing one ideal memristor via the Harmonic Balance Method (HBM). In Sec. 2 the considered class of circuits, which is composed of the interconnection of a linear time-invariant two-terminal (one port) element and a single ideal memelement, is described. Specifically, the linear element can contain linear R, L, C components and ideal operational amplifiers and controlled generators, while the memelement can be a flux- or charge-controlled memristor, a flux- or charge momentum-controlled capacitor, a flux momentum- or charge-controlled inductor. The problem of developing an input–output description of the considered class of circuits for each one of the six memelements is addressed in Sec. 3. It is shown that any circuit can be equivalently represented via a canonical reduced-order input–output system, thus implying that the circuit dynamics admits a first integral. Specifically, the reduced-order system is composed of an internal feedback interconnection between a linear dynamical subsystem and a nonlinear memoryless one, plus a feedforward linear dynamical subsystem driven by an external constant input. It turns out that the linear subsystems are characterized by either the impedance or the admittance of the linear two-terminal element, while the nonlinear subsystem is described by the characteristic of the memelement. This again highlights that the flux-charge domain is the natural ground for obtaining the reduced-order representation. Section 4 relates the developed input–output representation with the state space one. Specifically, it is shown how for each considered circuit the relative invariant manifolds can be analytically computed via a suitable state space realization of either the impedance or the admittance of the linear two-terminal element. Section 5 considers the extension to the case when the linear two-terminal element also contains external generators, by showing that this simply requires to add feedforward linear dynamic subsystems to the canonical reduced-order input–output system developed in Sec. 3. Several examples are presented throughout the paper to illustrate the features of the proposed approach.

2. Class of Circuits Description and Problem Formulation

In this section, we introduce the considered class of circuits and formulate the problem of interest. The class of circuits is assumed to contain linear elements and one ideal memelement. Specifically, it is composed of a finite-dimensional causal linear time-invariant two-terminal (one port) element **L**, with voltage $v_{\mathbf{L}}$ and current $i_{\mathbf{L}}$, and an ideal memelement **ME**, with voltage v_M and current i_M, as described in Fig. 1. Clearly, we have $v_{\mathbf{L}} = v_M$ and $i_{\mathbf{L}} = -i_M$.

2.1. *The linear two-terminal element* L

The two-terminal element **L** can be either a passive circuit containing only linear resistors, capacitors and inductors or an active one including also ideal operational amplifiers and controlled generators. In both cases the impedance and admittance of **L** are real rational functions of the complex variable but in the passive case they are subject to some restriction (see Remark 2.1). The case where **L** also

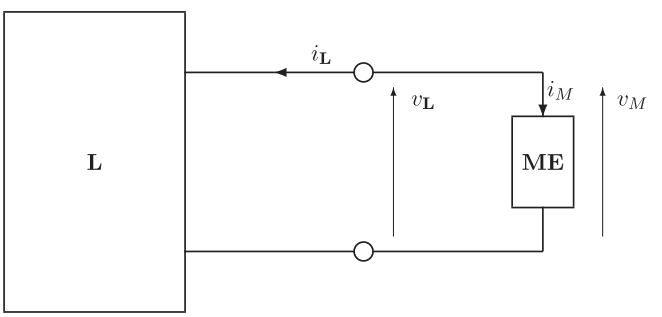

Fig. 1. The class of circuits.

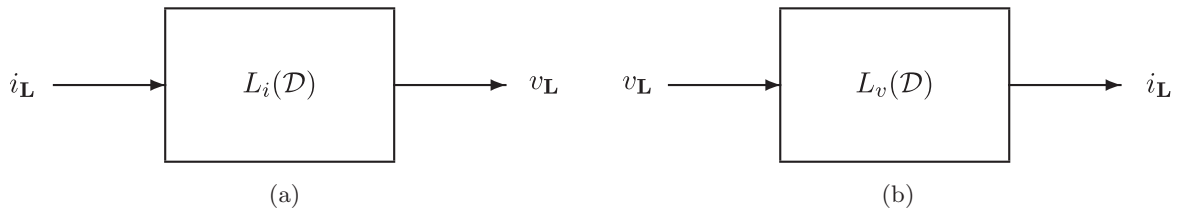

Fig. 2. (a) Current–voltage model $\mathcal{ML}_{i,v}$ and (b) voltage–current model $\mathcal{ML}_{v,i}$.

contains external generators will be considered in Sec. 5.

Two different finite-dimensional causal linear time-invariant input–output models can be adopted for $\mathbf{L}$: the current–voltage model $\mathcal{ML}_{i,v}$, where $i_{\mathbf{L}}$ and $v_{\mathbf{L}}$ are the input and the output of $\mathbf{L}$, respectively; the voltage–current model $\mathcal{ML}_{v,i}$, where $v_{\mathbf{L}}$ and $i_{\mathbf{L}}$ are the input and the output of $\mathbf{L}$, respectively. Models $\mathcal{ML}_{i,v}$ and $\mathcal{ML}_{v,i}$ are depicted in Fig. 2 and formally defined below, where $\mathcal{D}$ denotes the differential operator[1] (i.e. $\mathcal{D}f(t) = \dot{f}(t)$, $\mathcal{D}^2 f(t) = \ddot{f}(t)$, and so on).

Definition 2.1. The current–voltage model $\mathcal{ML}_{i,v}$ is described by input–output relation

$$v_{\mathbf{L}}(t) = L_i(\mathcal{D}) i_{\mathbf{L}}(t), \tag{1}$$

where

$$L_i(\mathcal{D}) = \frac{R_i(\mathcal{D})}{P_i(\mathcal{D})} \tag{2}$$

is a proper real rational function and $P_i(\mathcal{D})$, $R_i(\mathcal{D})$ are coprime polynomials of order n_i, i.e.

$$\begin{aligned} P_i(\mathcal{D}) &= \mathcal{D}^{n_i} + p_{n_i-1}\mathcal{D}^{n_i-1} + \cdots + p_1\mathcal{D} + p_0, \\ R_i(\mathcal{D}) &= r_{n_i}\mathcal{D}^{n_i} + r_{n_i-1}\mathcal{D}^{n_i-1} + \cdots + r_1\mathcal{D} + r_0. \end{aligned} \tag{3}$$

Definition 2.2. The voltage–current model $\mathcal{ML}_{v,i}$ is described by input–output relation

$$i_{\mathbf{L}}(t) = L_v(\mathcal{D}) v_{\mathbf{L}}(t), \tag{4}$$

where

$$L_v(\mathcal{D}) = \frac{R_v(\mathcal{D})}{P_v(\mathcal{D})} \tag{5}$$

is a proper real rational function and $P_v(\mathcal{D})$, $R_v(\mathcal{D})$ are coprime polynomials of order n_v, i.e.

$$\begin{aligned} P_v(\mathcal{D}) &= \mathcal{D}^{n_v} + p_{n_v-1}\mathcal{D}^{n_v-1} + \cdots + p_1\mathcal{D} + p_0, \\ R_v(\mathcal{D}) &= r_{n_v}\mathcal{D}^{n_v} + r_{n_v-1}\mathcal{D}^{n_v-1} + \cdots + r_1\mathcal{D} + r_0. \end{aligned} \tag{6}$$

Remark 2.1. If s denotes the complex variable, then $L_i(s)$ is exactly the equivalent impedance of $\mathbf{L}$, while $L_v(s)$ is the equivalent admittance. This implies that $L_i(\mathcal{D})$ and $L_v(\mathcal{D})$ are such that

$$L_i(\mathcal{D}) L_v(\mathcal{D}) = 1 \tag{7}$$

and, therefore, either only one between $L_i(\mathcal{D})$ and $L_v(\mathcal{D})$ is strictly proper, or $L_i(\mathcal{D})$ and $L_v(\mathcal{D})$ are both proper but not strictly proper. Moreover, if $\mathbf{L}$ is a passive circuit, i.e. it contains only resistors, capacitors and inductors, then the impedance $L_i(s)$ of $\mathcal{ML}_{i,v}$ and the admittance $L_v(s)$ of $\mathcal{ML}_{v,i}$ are constrained to be positive real [Khalil, 2002]. This implies that the relative degree of $L_i(s)$ and $L_v(s)$ cannot exceed one, i.e. $r_{n_i-1} \neq 0$ and $r_{n_v-1} \neq 0$. Hence, to have a relative degree greater than one $\mathbf{L}$ must be an active circuit, i.e. it must contain also ideal operational amplifiers and/or controlled generators.

Remark 2.2. Observe that Eqs. (1) and (4) can be equivalently written as $-v_{\mathbf{L}}(t) = L_i(\mathcal{D})(-i_{\mathbf{L}}(t))$ and $-i_{\mathbf{L}}(t) = L_v(\mathcal{D})(-v_{\mathbf{L}}(t))$, respectively. This formulation will be exploited in Sec. 4.

Remark 2.1 makes it clear when $\mathcal{ML}_{i,v}$ and $\mathcal{ML}_{v,i}$ can be used to ensure that $\mathbf{L}$ is a finite-dimensional causal linear time-invariant two-terminal element.

Proposition 1. *Let $L_i(\mathcal{D})$ be strictly proper, i.e. $r_{n_i} = 0$. Then, $\mathbf{L}$ is uniquely described by $\mathcal{ML}_{i,v}$ and $i_{\mathbf{L}}(t)$ and $v_{\mathbf{L}}(t)$ obey the following linear time-invariant ordinary differential equation*

$$P_i(\mathcal{D}) v_{\mathbf{L}}(t) - R_i(\mathcal{D}) i_{\mathbf{L}}(t) = 0. \tag{8}$$

Let $L_v(\mathcal{D})$ be strictly proper, i.e. $r_{n_v} = 0$. Then, $\mathbf{L}$ is uniquely described by $\mathcal{ML}_{v,i}$ and $v_{\mathbf{L}}(t)$ and $i_{\mathbf{L}}(t)$ obey the following linear time-invariant ordinary differential equation

$$P_v(\mathcal{D}) i_{\mathbf{L}}(t) - R_v(\mathcal{D}) v_{\mathbf{L}}(t) = 0. \tag{9}$$

[1]Throughout the paper, the inverse operator $\mathcal{D}^{-1}$ is the integral operator (i.e. $\mathcal{D}^{-1} f(t) = \int_{-\infty}^{t} f(\tau) d\tau$) and $\mathcal{D}^h f(t_0)$ stands for the value of $\mathcal{D}^h f(t)$ at $t = t_0$.

Let $L_i(\mathcal{D})$ and $L_v(\mathcal{D})$ be proper but not strictly proper, i.e. $r_{n_i} \neq 0$ and $r_{n_v} \neq 0$. Then, **L** *is described by both (8) and (9).*

The following assumption concerns the structural properties of controllability and observability enforced on **L**.

Assumption 2.1. Model $\mathcal{ML}_{i,v}$ is completely controllable and observable from input $i_{\mathbf{L}}$ and output $v_{\mathbf{L}}$. Model $\mathcal{ML}_{v,i}$ is completely controllable and observable from input $v_{\mathbf{L}}$ and output $i_{\mathbf{L}}$.

Remark 2.3. Assumption 2.1 ensures that the differential equations (8) and (9) completely describe the internal dynamics of **L**. In particular, it turns out that $\mathcal{ML}_{i,v}$ and $\mathcal{ML}_{v,i}$ admit equivalent state space representations of orders n_i and n_v, respectively (see Sec. 4).

Some examples of passive or active **L** are reported in Fig. 3 and discussed below.

Example 2.1. Let us consider the passive two-terminal element of Fig. 3(a). It can be verified that

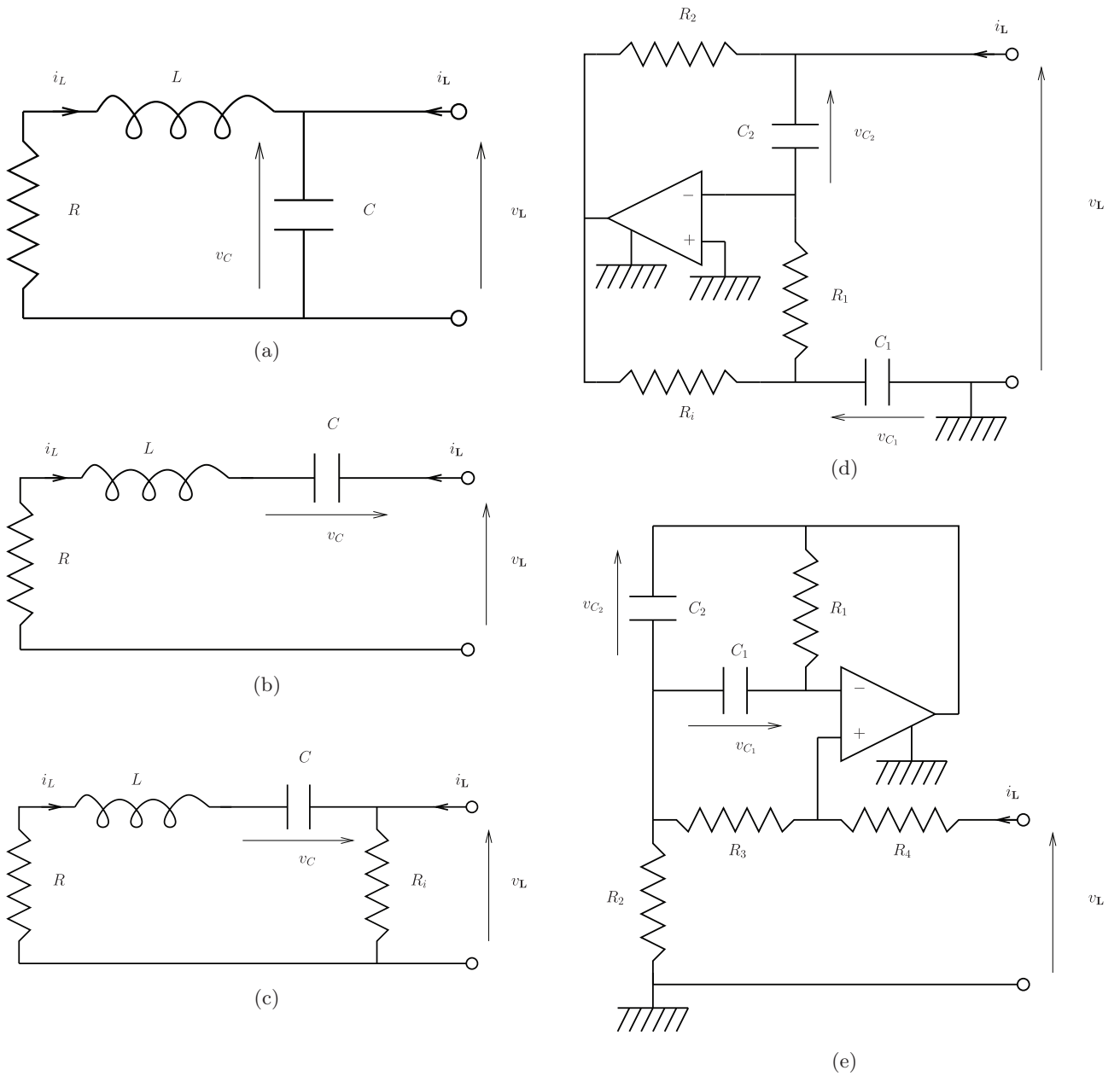

Fig. 3. Examples of (a)–(c) passive and (d) and (e) active two-terminal element **L**.

the equivalent impedance $L_i(s)$ is such that

$$L_i(\mathcal{D}) = \frac{\frac{1}{C}\mathcal{D} + \frac{R}{LC}}{\mathcal{D}^2 + \frac{R}{L}\mathcal{D} + \frac{1}{LC}}. \tag{10}$$

Hence, according to Proposition 1, $\mathbf{L}$ is modeled by the current–voltage model $\mathcal{ML}_{i,v}$ and the differential equation (8) becomes

$$\left(\mathcal{D}^2 + \frac{R}{L}\mathcal{D} + \frac{1}{LC}\right) v_{\mathbf{L}}(t) - \left(\frac{1}{C}\mathcal{D} + \frac{R}{LC}\right) i_{\mathbf{L}}(t) = 0. \tag{11}$$

Example 2.2. Consider the passive circuit of Fig. 3(b). It turns out that the equivalent admittance $L_v(s)$ is such that

$$L_v(\mathcal{D}) = \frac{\frac{1}{L}\mathcal{D}}{\mathcal{D}^2 + \frac{R}{L}\mathcal{D} + \frac{1}{LC}}. \tag{12}$$

Hence, according to Proposition 1, $\mathbf{L}$ is modeled by the voltage–current model $\mathcal{ML}_{v,i}$ and the differential equation (9) boils down to

$$\left(\mathcal{D}^2 + \frac{R}{L}\mathcal{D} + \frac{1}{LC}\right) i_{\mathbf{L}}(t) - \frac{1}{L}\mathcal{D} v_{\mathbf{L}}(t) = 0. \tag{13}$$

Example 2.3. For the passive circuit of Fig. 3(c), the equivalent impedance $L_i(s)$ and the equivalent admittance $L_v(s)$ of the network $\mathbf{L}$ are such that

$$L_i(\mathcal{D}) = \frac{R_i\mathcal{D}^2 + \frac{RR_i}{L}\mathcal{D} + \frac{R_i}{LC}}{\mathcal{D}^2 + \frac{R+R_i}{L}\mathcal{D} + \frac{1}{LC}}, \tag{14}$$

$$L_v(\mathcal{D}) = \frac{\frac{1}{R_i}\mathcal{D}^2 + \frac{R+R_i}{R_iL}\mathcal{D} + \frac{1}{R_iLC}}{\mathcal{D}^2 + \frac{R}{L}\mathcal{D} + \frac{1}{LC}}. \tag{15}$$

Hence, according to Proposition 1, $\mathbf{L}$ can be modeled by both $\mathcal{ML}_{i,v}$ and $\mathcal{ML}_{v,i}$ as

$$\left(\mathcal{D}^2 + \frac{R+R_i}{L}\mathcal{D} + \frac{1}{LC}\right) v_{\mathbf{L}}(t) - \left(R_i\mathcal{D}^2 + \frac{RR_i}{L}\mathcal{D} + \frac{R_i}{LC}\right) i_{\mathbf{L}}(t) = 0 \tag{16}$$

and

$$\left(\mathcal{D}^2 + \frac{R}{L}\mathcal{D} + \frac{1}{LC}\right) i_{\mathbf{L}}(t) - \left(\frac{1}{R_i}\mathcal{D}^2 + \frac{R+R_i}{R_iL}\mathcal{D} + \frac{1}{R_iLC}\right) v_{\mathbf{L}}(t) = 0, \tag{17}$$

respectively.

Example 2.4. The circuit of Fig. 3(d) is active since it contains one ideal operational amplifier. It can be verified that the equivalent impedance $L_i(s)$ is such that

$$L_i(\mathcal{D}) = \frac{\frac{R_2}{R_1R_iC_1C_2}}{\mathcal{D}^2 + \frac{R_1+R_2+R_i}{R_1R_iC_1}\mathcal{D} + \frac{1}{R_1R_iC_1C_2}}. \tag{18}$$

According to Proposition 1, in this case $\mathbf{L}$ is modeled by $\mathcal{ML}_{i,v}$ and (8) becomes

$$\left(\mathcal{D}^2 + \frac{R_1+R_2+R_i}{R_1R_iC_1}\mathcal{D} + \frac{1}{R_1R_iC_1C_2}\right) v_{\mathbf{L}}(t) - \frac{R_2}{R_1R_iC_1C_2} i_{\mathbf{L}}(t) = 0. \tag{19}$$

Example 2.5. Consider the active circuit of Fig. 3(e). In this case the equivalent admittance $L_v(s)$ is such that

$$L_v(\mathcal{D}) = \frac{\frac{1}{R_1R_2R_3C_1C_2}}{\mathcal{D}^2 + \frac{C_1+C_2}{R_1C_1C_2}\mathcal{D} + \frac{R_2+R_3+R_4}{R_1R_2R_3C_1C_2}}. \tag{20}$$

Hence, according to Proposition 1, $\mathbf{L}$ is modeled by $\mathcal{ML}_{v,i}$ and (9) becomes

$$\left(\mathcal{D}^2 + \frac{C_1+C_2}{R_1C_1C_2}\mathcal{D} + \frac{R_2+R_3+R_4}{R_1R_2R_3C_1C_2}\right) i_{\mathbf{L}}(t) - \left(\frac{1}{R_1R_2R_3C_1C_2}\right) v_{\mathbf{L}}(t) = 0. \tag{21}$$

2.2. *The memelement* ME

The memelement **ME** in Fig. 1 can be any of the following six memelements [Chua, 2009 (reaffirmed 2013); Corinto *et al.*, 2019]: (1) a flux-controlled memristor $\mathbf{MR}_{\varphi}$; (2) a charge-controlled

memristor $\mathbf{MR}_q$; (3) a flux-controlled memcapacitor $\mathbf{MC}_\varphi$; (4) a σ-controlled memcapacitor $\mathbf{MC}_\sigma$; (5) a charge-controlled meminductor $\mathbf{ML}_q$; (6) a ρ-controlled meminductor $\mathbf{ML}_\rho$. The definitions of these memelements are recalled below and involve the flux φ_M, the charge q_M as well as their time integrals. The time integral of the flux (or flux momentum) is defined as

$$\rho_M(t) = \int_{-\infty}^{t} \varphi_M(\tau)d\tau = \mathcal{D}^{-1}\varphi_M(t) \tag{22}$$

and in the differential form

$$\varphi_M(t) = \mathcal{D}\rho_M(t). \tag{23}$$

Analogously, the time integral of the charge (or charge momentum) is defined as

$$\sigma_M(t) = \int_{-\infty}^{t} q_M(\tau)d\tau = \mathcal{D}^{-1}q_M(t) \tag{24}$$

and in the differential form

$$q_M(t) = \mathcal{D}\sigma_M(t). \tag{25}$$

• A flux-controlled memristor $\mathbf{MR}_\varphi$ is described by the nonlinear flux-charge characteristic $\hat{q} : \mathbb{R} \to \mathbb{R}$ relating the flux φ_M and the charge q_M as follows:

$$q_M = \hat{q}(\varphi_M). \tag{26}$$

In the voltage–current domain the dynamics of $\mathbf{MR}_\varphi$ obeys

$$\begin{cases} \mathcal{D}\varphi_M(t) = v_M(t), \\ i_M(t) = \hat{q}'(\varphi_M(t))v_M(t), \end{cases} \tag{27}$$

where the derivative $\hat{q}'(\varphi_M)$ is known as the memconductance of the memristor. Note that $\mathbf{MR}_\varphi$ is modeled by a first order causal time-invariant nonlinear system with input v_M, output i_M and state φ_M. The block diagram representation of (27) is depicted in Fig. 4(a).

• A charge-controlled memristor $\mathbf{MR}_q$ is described by the nonlinear charge-flux characteristic $\hat{\varphi} : \mathbb{R} \to \mathbb{R}$ relating the charge q_M and the flux φ_M as follows:

$$\varphi_M = \hat{\varphi}(q_M). \tag{28}$$

In the voltage–current domain the dynamics of $\mathbf{MR}_q$ obeys

$$\begin{cases} \mathcal{D}q_M(t) = i_M(t), \\ v_M(t) = \hat{\varphi}'(q_M(t))i_M(t), \end{cases} \tag{29}$$

where the derivative $\hat{\varphi}'(q_M)$ is known as the memristance of the memristor. Note that $\mathbf{MR}_q$ is modeled by a first order causal time-invariant nonlinear system with input i_M, output v_M and state q_M. The block diagram representation of (29) is depicted in Fig. 4(b).

• A flux-controlled memcapacitor $\mathbf{MC}_\varphi$ is characterized by the nonlinear characteristic $\hat{\sigma} : \mathbb{R} \to \mathbb{R}$ relating the flux φ_M and the charge momentum σ_M as follows:

$$\sigma_M = \hat{\sigma}(\varphi_M). \tag{30}$$

In the voltage–current domain $\mathbf{MC}_\varphi$ obeys

$$\begin{cases} \mathcal{D}\varphi_M(t) = v_M(t), \\ q_M(t) = \hat{\sigma}'(\varphi_M(t))v_M(t), \\ i_M(t) = \mathcal{D}q_M(t), \end{cases} \tag{31}$$

where the derivative $\hat{\sigma}'(\varphi_M)$ is known as the memcapacitance of $\mathbf{MC}_\varphi$. Note that the first

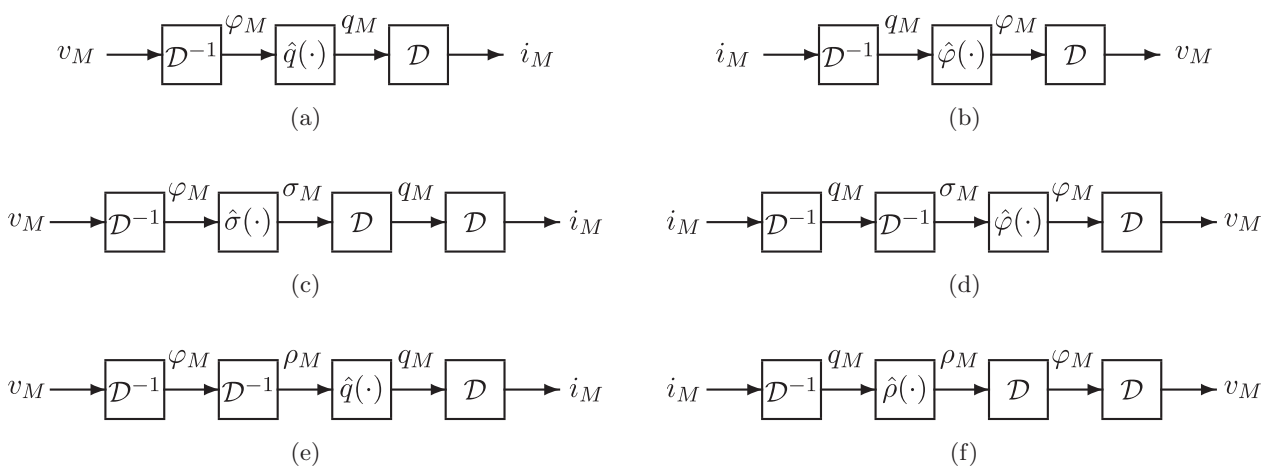

Fig. 4. Block diagram representations: (a) $\mathbf{MR}_\varphi$, (b) $\mathbf{MR}_q$, (c) $\mathbf{MC}_\varphi$, (d) $\mathbf{MC}_\sigma$, (e) $\mathbf{ML}_\rho$ and (f) $\mathbf{ML}_q$.

two equations represent a first order causal time-invariant nonlinear system with input v_M, output q_M and state φ_M, while the third equation provides i_M as the output of a pure derivative system with input q_M. The block diagram representation of (31) is depicted in Fig. 4(c).

• A σ-controlled memcapacitor $\mathbf{MC}_\sigma$ is described by the nonlinear characteristic $\hat{\varphi} : \mathbb{R} \to \mathbb{R}$ relating the charge momentum σ_M and the flux φ_M as follows:

$$\varphi_M = \hat{\varphi}(\sigma_M). \tag{32}$$

In the voltage–current domain the dynamics of $\mathbf{MC}_\sigma$ obeys

$$\begin{cases} \mathcal{D}\sigma_M(t) = q_M(t), \\ \mathcal{D}q_M(t) = i_M(t), \\ v_M(t) = \hat{\varphi}'(\sigma_M(t))q_M(t), \end{cases} \tag{33}$$

where the derivative $\hat{\varphi}'(\sigma_M)$ is known as the inverse memcapacitance of $\mathbf{MC}_\sigma$. Note that $\mathbf{MC}_\sigma$ is modeled by a second order causal time-invariant nonlinear system with input i_M, output v_M and state variables σ_M and q_M. The block diagram representation of (33) is depicted in Fig. 4(d).

• A ρ-controlled meminductor $\mathbf{ML}_\rho$ is characterized by the nonlinear characteristic $\hat{q} : \mathbb{R} \to \mathbb{R}$ relating the flux momentum ρ_M and the charge q_M as follows:

$$q_M = \hat{q}(\rho_M). \tag{34}$$

In the voltage–current domain $\mathbf{ML}_\rho$ obeys

$$\begin{cases} \mathcal{D}\rho_M(t) = \varphi_M(t), \\ \mathcal{D}\varphi_M(t) = v_M(t), \\ i_M(t) = \hat{q}'(\rho_M(t))\varphi_M(t), \end{cases} \tag{35}$$

where the derivative $\hat{q}'(\rho_M)$ is known as the inverse meminductance of $\mathbf{ML}_\rho$. Note that $\mathbf{ML}_\rho$ is modeled by a second order causal time-invariant nonlinear system with input v_M, output i_M and state variables ρ_M and φ_M. The block diagram representation of (35) is depicted in Fig. 4(e).

• A charge-controlled meminductor $\mathbf{ML}_q$ is characterized by the nonlinear characteristic $\hat{\rho} : \mathbb{R} \to \mathbb{R}$ relating the charge q_M and the flux momentum ρ_M as follows:

$$\rho_M = \hat{\rho}(q_M). \tag{36}$$

In the voltage–current domain $\mathbf{ML}_q$ obeys

$$\begin{cases} \mathcal{D}q_M(t) = i_M(t), \\ \varphi_M(t) = \hat{\rho}'(q_M(t))i_M(t), \\ v_M(t) = \mathcal{D}\varphi_M(t), \end{cases} \tag{37}$$

where the derivative $\hat{\rho}'(q_M)$ is known as the meminductance of $\mathbf{ML}_q$. Note that the first two equations represent a first order causal time-invariant nonlinear system with input i_M, output φ_M and state q_M, while the third equation provides v_M as the output of a pure derivative system with input φ_M. The block diagram representation of (37) is depicted in Fig. 4(f).

Throughout the paper, it is assumed that the nonlinear characteristics (26), (28), (30), (32), (34), (36) vanish as the argument is equal to zero. Also, it is enforced that they are as smooth as needed to ensure existence and uniqueness of the solutions of the system of differential equations describing the dynamics of the class of circuits of Fig. 1.

2.3. *Problem formulation*

We are interested in studying the dynamics of the class of circuits of Fig. 1 where **ME** can be any of the six memelements considered in Sec. 2.2. In this respect, from Fig. 4 it follows that the input and the output of each **ME** are clearly well defined. This implies that, since $v_{\mathbf{L}} = v_M$ and $i_{\mathbf{L}} = -i_M$, the class of circuits of Fig. 1 admits six input–output feedback representations in the voltage–current domain, each one pertaining to a given memelement. Specifically, the representations correspond to interconnecting the memelements $\mathbf{MR}_\varphi$, $\mathbf{MC}_\varphi$ and $\mathbf{ML}_\rho$ with the current–voltage model $\mathcal{ML}_{i,v}$ [see Fig. 5(a)] and the memelements $\mathbf{MR}_q$, $\mathbf{MC}_\sigma$ and $\mathbf{ML}_q$ with the voltage–current model $\mathcal{ML}_{v,i}$ [see Fig. 5(b)]. Note that for the systems of Fig. 5(b) the input and the output of $\mathcal{ML}_{v,i}$ are indeed $-v_{\mathbf{L}}$ and $-i_{\mathbf{L}}$ (see also Remark 2.2), respectively. Clearly, the dynamics of each representation is completely described by either the differential equation (8) or the differential equation (9) plus the dynamical relations pertaining to the considered memelement **ME** [i.e. (27) for $\mathbf{MR}_\varphi$, (29) for $\mathbf{MR}_q$, (31) for $\mathbf{MC}_\varphi$ and so on].

Our aim is to find the most simple input–output description of the dynamics displayed by each one of the six representations of Fig. 5. In Sec. 3, we show how a canonical reduced order input–output

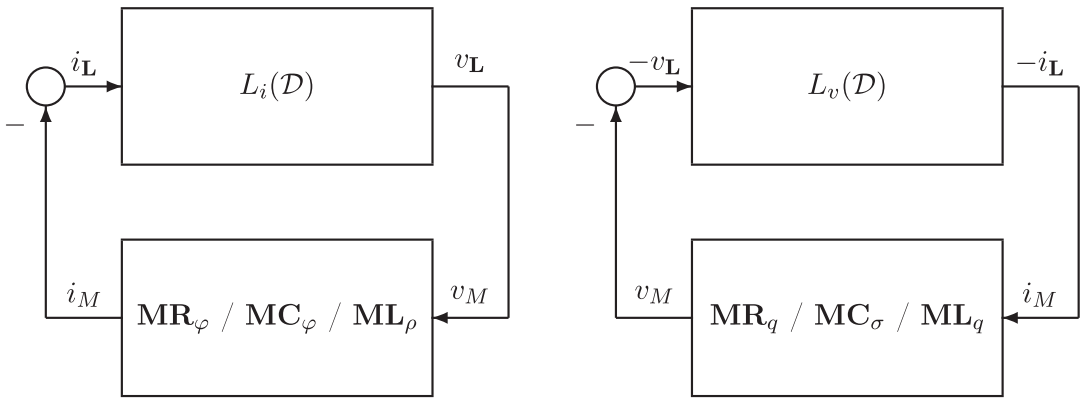

Fig. 5. Input–output feedback representations in the voltage–current domain: (a) $\mathcal{ML}_{i,v}$ with $\mathbf{MR}_\varphi$, $\mathbf{MC}_\varphi$ and $\mathbf{ML}_\rho$ and (b) $\mathcal{ML}_{v,i}$ with $\mathbf{MR}_q$, $\mathbf{MC}_\sigma$ and $\mathbf{ML}_q$.

representation, able to completely describe the sought dynamics, can be found in the flux-charge domain. Specifically, the dynamics of each one of the six representations of Fig. 5 can be exactly obtained by collecting the dynamics of a family of reduced order nonlinear differential equations involving only the variable used for controlling the memelement, i.e. the flux φ_M for both $\mathbf{MR}_\varphi$ and $\mathbf{MC}_\varphi$, the charge q_M for both $\mathbf{MR}_q$ and $\mathbf{ML}_q$, the flux momentum ρ_M for $\mathbf{ML}_\rho$ and the charge momentum σ_M for $\mathbf{MC}_\sigma$. The relation of this input–output approach with the state space one developed in [Corinto *et al.*, 2019] is discussed in Sec. 4. Finally, Sec. 5 deals with the extension to the case where $\mathbf{L}$ also contains generators.

3. A Canonical Reduced Order Input–Output Representation of the Class of Circuits

In this section, we focus on the possibility of describing the dynamics of each one of the six feedback representations of Fig. 5 via that of the canonical input–output system Σ depicted in Fig. 6, where the external input r is assumed to be any constant value (i.e. $r(t) = X_0$, $X_0 \in \mathbb{R}$). It is worth observing that Σ has an internal feedback interconnection between the linear subsystem $L_1(\mathcal{D})$ and the nonlinear subsystem described by the function $n(\cdot)$, while $L_2(\mathcal{D})$ is a feedforward linear block driven by the external constant input r. A lot of attention has been devoted in the literature to the study of dynamical properties of systems enjoying this structure, due to its connection with the celebrated Lur'e control problem (see e.g. [Khalil, 2002]).

Specifically, in the next three subsections, we show that each one of the six feedback representations of Fig. 5 admits an equivalent description via the canonical system Σ, where the system output y and the nonlinear function $n(\cdot)$ of Σ are the controlling variable and the nonlinear characteristic of the considered **ME** (i.e. the flux φ_M and the flux-charge characteristic $\hat{q}$ for $\mathbf{MR}_\varphi$, and so on), while the rational functions $L_1(\mathcal{D})$ and $L_2(\mathcal{D})$ depend on $L_i(\mathcal{D})$ for the feedback interconnections of Fig. 5(a) and $L_v(\mathcal{D})$ for those of Fig. 5(b). Memristors $\mathbf{MR}_\varphi$ and $\mathbf{MR}_q$ are considered in Sec. 3.1, while Sec. 3.2 deals with $\mathbf{MC}_\varphi$ and $\mathbf{MC}_\sigma$ and Sec. 3.3 is devoted to $\mathbf{ML}_q$ and $\mathbf{ML}_\rho$. Finally, Sec. 3.4 summarizes the obtained results.

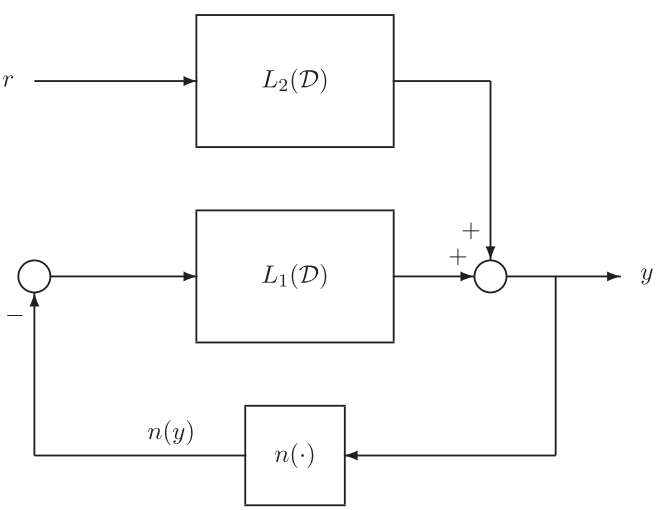

Fig. 6. System Σ: a canonical input–output representation of the class of circuits.

3.1. *The case of ideal memristor*

Consider the class of circuits of Fig. 1 with $\mathbf{MR}_\varphi$ as **ME**. Exploiting (8) and (27), it turns out that the relative representation of Fig. 5(a) is governed by the system of differential equations

$$\begin{cases} P_i(\mathcal{D})v_M(t) + R_i(\mathcal{D})i_M(t) = 0, \\ \mathcal{D}\varphi_M(t) = v_M(t), \end{cases} \tag{38}$$

with i_M as in the second equation of (27). The next result holds true.

Proposition 2. *Consider the class of circuits of Fig. 1 with* $\mathbf{MR}_\varphi$ *as* **ME** *and* **L** *such that* $L_i(\mathcal{D})$ *is strictly proper, i.e.* $r_{n_i} = 0$*, and let Assumption 2.1 hold. Then, the dynamics of the class of circuits is completely described by the one-parameter family of differential equations of order* n_i

$$\Sigma_{\Phi_0^{(R)}}: \begin{cases} P_i(\mathcal{D})\varphi_M(t) + R_i(\mathcal{D})\hat{q}(\varphi_M(t)) = \Phi_0^{(R)}, \\ \Phi_0^{(R)} \in \mathbb{R}. \end{cases} \tag{39}$$

Proof. We first observe that Assumption 2.1 ensures that (38) completely describes the internal dynamics of the considered class of circuits. Then, since $i_M = \mathcal{D}q_M$, it can be verified that the system of differential equations (38) is equivalent to the following single differential equation of order $n_i + 1$

$$P_i(\mathcal{D})\mathcal{D}\varphi_M(t) + R_i(\mathcal{D})\mathcal{D}q_M(t) = 0, \tag{40}$$

where $q_M(t) = \hat{q}(\varphi_M(t))$ according to (26). Moreover, the condition $r_{n_i} = 0$ ensures that the solutions of (40), and hence of (38), are uniquely determined by the initial conditions $\varphi_M(t_0), v_M(t_0), \mathcal{D}v_M(t_0), \ldots, \mathcal{D}^{n_i-1}v_M(t_0)$. Now, it turns out that (40) can be equivalently rewritten as

$$\mathcal{D}(P_i(\mathcal{D})\varphi_M(t) + R_i(\mathcal{D})q_M(t)) = 0. \tag{41}$$

This implies that the scalar variable

$$\begin{aligned} \Phi^{(R)}(t) &\doteq P_i(\mathcal{D})\varphi_M(t) + R_i(\mathcal{D})q_M(t) \\ &= P_i(\mathcal{D})\varphi_M(t) + R_i(\mathcal{D})\hat{q}(\varphi_M(t)) \end{aligned} \tag{42}$$

is constant over time, i.e.

$$\Phi^{(R)}(t) = \Phi^{(R)}(t_0) \doteq \Phi_0^{(R)} \quad \forall\, t \geq t_0, \tag{43}$$

which is exactly the differential equation defining $\Sigma_{\Phi_0^{(R)}}$. To complete the proof, it remains to show that $\Phi_0^{(R)}$ must assume any real value to ensure that $\Sigma_{\Phi_0^{(R)}}$ generates all the solutions of the system of differential equations (38). Observe that $\Phi_0^{(R)}$ depends on the initial conditions $\varphi_M(t_0), v_M(t_0), \mathcal{D}v_M(t_0), \ldots, \mathcal{D}^{n_i-1}v_M(t_0)$ of (38) as follows

$$\begin{aligned} \Phi_0^{(R)} = \mathcal{D}^{n_i-1}v_M(t_0) &+ \sum_{h=0}^{n_i-2} p_{h+1}\mathcal{D}^h v_M(t_0) \\ &+ p_0\varphi_M(t_0) + \sum_{h=0}^{n_i-1} r_h\mathcal{D}^h\hat{q}(\varphi_M(t_0)). \end{aligned} \tag{44}$$

Also, it can be verified that $\sum_{h=0}^{n_i-1} r_h\mathcal{D}^h\hat{q}(\varphi_M(t_0))$ does not depend on $\mathcal{D}^{n_i-1}v_M(t_0)$ but only on $\varphi_M(t_0)$, $v_M(t_0)$, $\mathcal{D}v_M(t_0), \ldots, \mathcal{D}^{n_i-2}v_M(t_0)$, and hence $\Phi_0^{(R)}$ can be written as

$$\begin{aligned} \Phi_0^{(R)} = \mathcal{D}^{n_i-1}v_M(t_0) &+ F_\varphi(\varphi_M(t_0), v_M(t_0), \\ &\mathcal{D}v_M(t_0), \ldots, \mathcal{D}^{n_i-2}v_M(t_0)) \end{aligned} \tag{45}$$

with

$$\begin{aligned} &F_\varphi(\varphi_M(t_0), v_M(t_0), \mathcal{D}v_M(t_0), \ldots, \mathcal{D}^{n_i-2}v_M(t_0)) \\ &\quad\doteq \sum_{h=0}^{n_i-2} p_{h+1}\mathcal{D}^h v_M(t_0) + p_0\varphi_M(t_0) \\ &\qquad + \sum_{h=0}^{n_i-1} r_h\mathcal{D}^h\hat{q}(\varphi_M(t_0)). \end{aligned} \tag{46}$$

This implies that the solution of $\Sigma_{\Phi_0^{(R)}}$ with initial conditions $\varphi_M(t_0)$, $v_M(t_0)$, $\mathcal{D}v_M(t_0), \ldots, \mathcal{D}^{n_i-2}v_M(t_0)$ is exactly the solution of the system of differential equations (38) with initial conditions $\varphi_M(t_0)$, $v_M(t_0)$, $\mathcal{D}v_M(t_0)$, $\ldots$, $\mathcal{D}^{n_i-1}v_M(t_0)$ once

$$\begin{aligned} \mathcal{D}^{n_i-1}v_M(t_0) = \Phi_0^{(R)} &- F_\varphi(\varphi_M(t_0), v_M(t_0), \\ &\mathcal{D}v_M(t_0), \ldots, \mathcal{D}^{n_i-2}v_M(t_0)), \end{aligned} \tag{47}$$

which in turn shows that $\Phi_0^{(R)}$ must assume any real value. ■

Remark 3.1. The proof makes it clear that (38) admits a first integral and thus its dynamics is confined to lie in some invariant manifold according to Eqs. (42) and (43). Indeed, this fact is related to the well-known property that the state space of circuits containing an ideal memelement is foliated, as it will be discussed in Sec. 4.

Remark 3.2. Note that $\Sigma_{\Phi_0^{(R)}}$ can be equivalently described by the input–output relation

$$\varphi_M(t) = -L_i(\mathcal{D})\hat{q}(\varphi_M(t)) + \frac{1}{P_i(\mathcal{D})}\Phi_0^{(R)}, \qquad \Phi_0^{(R)} \in \mathbb{R}, \tag{48}$$

thus implying that $\Sigma_{\Phi_0^{(R)}}$ admits the canonical input–output representation of Fig. 6 once

$$y = \varphi_M, \quad n(\cdot) = \hat{q}(\cdot), \quad n(y) = q_M,$$
$$L_1(\mathcal{D}) = L_i(\mathcal{D}), \quad L_2(\mathcal{D}) = \frac{1}{P_i(\mathcal{D})}, \quad r = \Phi_0^{(R)}. \tag{49}$$

In addition, it can be shown that this representation is exactly that of a circuit containing a nonlinear resistor in place of the memristor plus an additional constant generator (see, e.g. Example 3.1).

Consider now the class of circuits of Fig. 1 with $\mathbf{MR}_q$ as **ME**. Exploiting (9) and (29), it follows that the dynamics of the relative representation of Fig. 5(b) is governed by

$$\begin{cases} P_v(\mathcal{D})i_M(t) + R_v(\mathcal{D})v_M(t) = 0, \\ \mathcal{D}q_M(t) = i_M(t), \end{cases} \tag{50}$$

with v_M as in the second equation of (29). In this case, the following result holds.

Proposition 3. *Consider the class of circuits of Fig. 1 with* $\mathbf{MR}_q$ *as* **ME** *and* **L** *such that* $L_v(\mathcal{D})$ *is strictly proper, i.e.* $r_{n_v} = 0$*, and let Assumption 2.1 hold. Then, the dynamics of the class of circuits is completely described by the one-parameter family of differential equations of order* n_v

$$\Sigma_{Q_0^{(R)}}: \begin{cases} P_v(\mathcal{D})q_M(t) + R_v(\mathcal{D})\hat{\varphi}(q_M(t)) = Q_0^{(R)}, \\ Q_0^{(R)} \in \mathbb{R}. \end{cases} \tag{51}$$

Proof. The proof parallels that of Proposition 2 once i_M, v_M, q_M, φ_M, $L_i(\mathcal{D})$ and $\hat{q}(\cdot)$ are replaced with v_M, i_M, φ_M, q_M, $L_v(\mathcal{D})$ and $\hat{\varphi}(\cdot)$, respectively. In particular, it turns out that the scalar variable

$$Q^{(R)}(t) \doteq P_v(\mathcal{D})q_M(t) + R_v(\mathcal{D})\varphi_M(t) = P_v(\mathcal{D})q_M(t) + R_v(\mathcal{D})\hat{\varphi}(q_M(t)) \tag{52}$$

is constant over time, i.e.

$$Q^{(R)}(t) = Q^{(R)}(t_0) \doteq Q_0^{(R)} \quad \forall\, t \geq t_0, \tag{53}$$

where the constant $Q_0^{(R)}$ is given by the sum of the initial conditions $\mathcal{D}^{n_v-1}i_M(t_0)$ and a term depending only on the remaining initial conditions $q_M(t_0)$, $i_M(t_0), \mathcal{D}i_M(t_0), \ldots, \mathcal{D}^{n_v-2}i_M(t_0)$. ■

Remark 3.3. Note that also (50) admits a first integral. Moreover, $\Sigma_{Q_0^{(R)}}$ is equivalently described by the input–output relation

$$q_M(t) = -L_v(\mathcal{D})\hat{\varphi}(q_M(t)) + \frac{1}{P_v(\mathcal{D})}Q_0^{(R)}, \qquad Q_0^{(R)} \in \mathbb{R}. \tag{54}$$

This implies that $\Sigma_{Q_0^{(R)}}$ admits the canonical representation of Fig. 6 once

$$y = q_M, \quad n(\cdot) = \hat{\varphi}(\cdot), \quad n(y) = \varphi_M,$$
$$L_1(\mathcal{D}) = L_v(\mathcal{D}), \quad L_2(\mathcal{D}) = \frac{1}{P_v(\mathcal{D})}, \quad r = Q_0^{(R)}. \tag{55}$$

Also in this case, there exists a circuit containing a nonlinear resistor in place of the memristor plus an additional constant generator (see, e.g. Example 3.2).

From Proposition 2 (resp., Proposition 3) it turns out that, among the two-terminal elements of Fig. 3, $\mathbf{MR}_\varphi$ (resp., $\mathbf{MR}_q$) can be interconnected only with those of Figs. 3(a) and 3(d) [resp., Figs. 3(b) and 3(e)]. Three examples are now considered in some details: the first two deal with the cases of Figs. 3(a) and 3(b), the third one discusses why Propositions 2 and 3 do not apply to the case of Fig. 3(c).

Example 3.1. Consider the circuit of Fig. 3(a) with $\mathbf{MR}_\varphi$ as **ME**.[2] From (10) it follows that the reduced order family Σ_{Φ_0} in (39) amounts to

$$\left(\mathcal{D}^2 + \frac{R}{L}\mathcal{D} + \frac{1}{LC}\right)\varphi_M(t) + \left(\frac{1}{C}\mathcal{D} + \frac{R}{LC}\right)\hat{q}(\varphi_M(t)) = \Phi_0^{(R)}, \tag{56}$$

where the parameter $\Phi_0^{(R)}$ is any real number. Proposition 2 ensures that each solution of the

[2]This circuit is the unforced version of the well-known Murali–Lakshmanan–Chua oscillatory memristive circuit (see, e.g. [Ahamed & Lakshmanan, 2017]).

system of differential equations (38) can be recovered as a solution of (56) for a specific value of $\Phi_0^{(R)}$. Indeed, let $v_M(t)$ and $\varphi_M(t)$ be the solution of (38), i.e.

$$\begin{cases} \left(\mathcal{D}^2 + \dfrac{R}{L}\mathcal{D} + \dfrac{1}{LC}\right) v_M(t) \\ \qquad + \left(\dfrac{1}{C}\mathcal{D} + \dfrac{R}{LC}\right) i_M(t) = 0, \\ \mathcal{D}\varphi_M(t) = v_M(t), \end{cases} \tag{57}$$

with $i_M(t)$ as in the second equation of (27) and initial conditions $v_M(t_0)$, $\mathcal{D}v_M(t_0)$ and $\varphi_M(t_0)$. Then, it can be checked that this solution is exactly the solution of the second order differential equation in (56), once $\Phi_0^{(R)}$ is given by

$$\Phi_0^{(R)} = \mathcal{D}v_M(t_0) + \frac{R}{L}v_M(t_0) + \frac{1}{LC}\varphi_M(t_0) + \frac{R}{LC}\hat{q}(\varphi_M(t_0)) + \frac{1}{C}\mathcal{D}\hat{q}(\varphi_M(t_0)). \tag{58}$$

Moreover, it turns out that the dynamics of (56) is exactly that displayed by the circuit of Fig. 7(a) where V is a constant voltage generator and the memristor is replaced by a nonlinear resistor with voltage–current characteristic $\hat{g}(\cdot)$, i.e. $i_{RNL} = \hat{g}(v_{RNL})$. Indeed, it can be verified that the dynamics of this circuit obeys the following differential equation

$$\left(\mathcal{D}^2 + \frac{R}{L}\mathcal{D} + \frac{1}{LC}\right) v_{RNL}(t) + \left(\frac{1}{C}\mathcal{D} + \frac{R}{LC}\right) \hat{g}(v_{RNL}(t)) = \frac{V}{LC}, \tag{59}$$

which exactly coincides with (56) once $V = \Phi_0^{(R)} LC$, $v_{RNL} = \varphi_M$ and $\hat{q}(\cdot) = \hat{g}(\cdot)$.

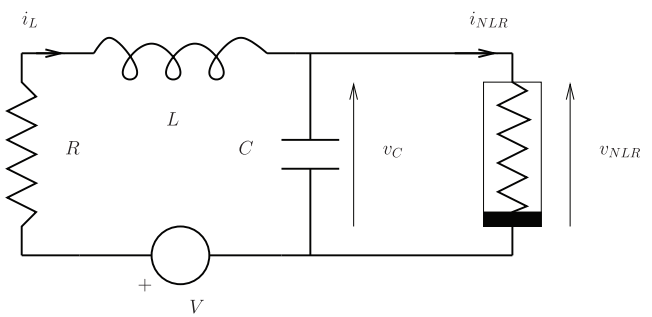

(a)

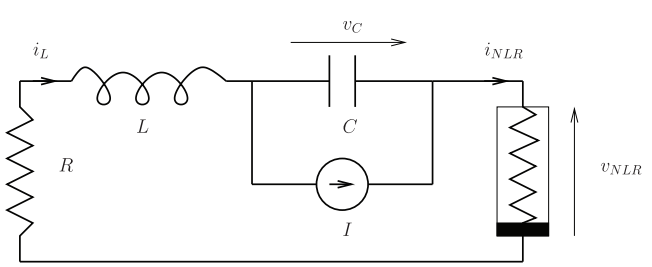

(b)

Fig. 7. Equivalent circuits with nonlinear resistors and additional constant generators of the memristor circuits: (a) Example 3.1 and (b) Example 3.2.

Example 3.2. Consider the circuit of Fig. 3(b) with $\mathbf{MR}_q$ as **ME**. From (12) the family $\Sigma_{Q_0^{(R)}}$ in (51) is given by

$$\left(\mathcal{D}^2 + \frac{R}{L}\mathcal{D} + \frac{1}{LC}\right) q_M(t) + \frac{1}{L}\mathcal{D}\hat{\varphi}(q_M(t)) = Q_0^{(R)}, \tag{60}$$

with $Q_0^{(R)} \in \mathbb{R}$. Also in this case the dynamics of (60) can be exactly recovered by the circuit of Fig. 7(b), where I is a constant current generator and the memristor is replaced by a nonlinear resistor with current–voltage characteristic $\hat{r}(\cdot)$, i.e. $v_{RNL} = \hat{r}(i_{RNL})$. Indeed, the dynamics of the circuits obeys

$$\left(\mathcal{D}^2 + \frac{R}{L}\mathcal{D} + \frac{1}{LC}\right) i_{RNL}(t) + \frac{1}{L}\mathcal{D}\hat{r}(i_{RNL}(t)(t)) = \frac{I}{LC}, \tag{61}$$

which is equal to (60) once $I = Q_0^{(R)} LC$, $i_{RNL} = q_M$ and $\hat{\varphi}(\cdot) = \hat{r}(\cdot)$.

Example 3.3. Consider the circuit of Fig. 3(c) with $\mathbf{MR}_\varphi$ as **ME**. It turns out that $L_i(\mathcal{D})$ is proper but not strictly proper and the differential equation (8) becomes

$$\left(\mathcal{D}^2 + \frac{R + R_i}{L}\mathcal{D} + \frac{1}{LC}\right) v_{\mathbf{L}}(t) - \left(R_i\mathcal{D}^2 + \frac{RR_i}{L}\mathcal{D} + \frac{R_i}{LC}\right) i_{\mathbf{L}}(t) = 0. \tag{62}$$

It can be readily verified that the dynamics of the circuit is described by the differential equation

$$\left(\mathcal{D}^2 + \frac{R + R_i}{L}\mathcal{D} + \frac{1}{LC}\right) \mathcal{D}\varphi_M(t) + \left(R_i\mathcal{D}^2 + \frac{RR_i}{L}\mathcal{D} + \frac{R_i}{LC}\right) \mathcal{D}\hat{q}(\varphi_M(t)) = 0, \tag{63}$$

whose solutions are uniquely determined once the initial conditions $\varphi_M(t_0)$, $v_M(t_0)$ and $\mathcal{D}v_M(t_0)$ are fixed. Now, (63) can be equivalently rewritten as

$$\mathcal{D}\left(\left(\mathcal{D}^2+\frac{R+R_i}{L}\mathcal{D}+\frac{1}{LC}\right)\varphi_M(t) + \left(R_i\mathcal{D}^2+\frac{RR_i}{L}\mathcal{D}+\frac{R_i}{LC}\right)\hat{q}(\varphi_M(t))\right)=0, \tag{64}$$

from which it follows that

$$\left(\mathcal{D}^2+\frac{R+R_i}{L}\mathcal{D}+\frac{1}{LC}\right)\varphi_M(t) + \left(R_i\mathcal{D}^2+\frac{RR_i}{L}\mathcal{D}+\frac{R_i}{LC}\right)\hat{q}(\varphi_M(t)) = \Phi_0^{(R)} \quad \forall\, t\geq t_0, \tag{65}$$

with

$$\begin{aligned}\Phi_0^{(R)} &= (1+R_i\hat{q}'(\varphi_M(t_0)))\mathcal{D}v_M(t_0) + \frac{1}{LC}(\varphi_M(t_0)+R_i\hat{q}(\varphi_M(t_0))) \\ &\quad + \left(\frac{R+R_i}{L}+\frac{RR_i}{L}\hat{q}'(\varphi_M(t_0)) + R_i\hat{q}''(\varphi_M(t_0))v_M(t_0)\right)v_M(t_0).\end{aligned} \tag{66}$$

Hence, the differential equation (63) still admits a first integral. However, (66) shows that, differently from the case when $L_i(\mathcal{D})$ is strictly proper as in the proof of Proposition 2, for fixed $\varphi_M(t_0)$ and $v_M(t_0)$ the relation between $\Phi_0^{(R)}$ and $\mathcal{D}v_M(t_0)$ is not in general invertible. Indeed, the family of differential equations (65) generates all the solutions of (63) by varying $\Phi_0^{(R)}\in\mathbb{R}$ once $\hat{q}(\cdot)$ and R_i are such that $1+R_i\hat{q}'(\phi)\neq 0$, $\forall\,\phi\in\mathbb{R}$. It can be shown that this condition is related to the well-known impasse point issue, which prevents the existence of a state space representation for the circuit (see, e.g. [Chua, 1980]). Clearly, the same conclusion can be reached by considering the circuit of Fig. 3(c) with $\mathbf{MR}_q$ as **ME**.

Remark 3.4. Example 3.3 makes it clear that if $L_i(\mathcal{D})$ (resp., $L_v(\mathcal{D})$) is not strictly proper, then $\Sigma_{\Phi_0^{(R)}}$ (resp., $\Sigma_{Q_0^{(R)}}$) does not provide an equivalent representation of (38) [resp., (50)] for all the nonlinear characteristics (26) [resp., (28)], but only for some of them.

3.2. *The case of ideal memcapacitor*

Consider the class of circuits of Fig. 1 with $\mathbf{MC}_\varphi$ as **ME**. In this case, the dynamics of the corresponding representation of Fig. 5(a) is governed by

$$\begin{cases}P_i(\mathcal{D})v_M(t)+R_i(\mathcal{D})i_M(t)=0,\\ \mathcal{D}\varphi_M(t)=v_M(t),\end{cases} \tag{67}$$

where i_M is obtained from φ_M and v_M according to the second and third equations in (31). We have the following result.

Proposition 4. *Consider the class of circuits of Fig. 1 with* $\mathbf{MC}_\varphi$ *as* **ME** *and* $\mathbf{L}$ *such that* $L_i(\mathcal{D})$ *has relative degree greater than one, i.e.* $r_{n_i}=r_{n_i-1}=0$, *and let Assumption 2.1 hold. Then, the dynamics of the class of circuits is completely described by the one-parameter family of differential equations of order* n_i

$$\Sigma_{\Phi_0^{(C)}}:\ \begin{cases}P_i(\mathcal{D})\varphi_M(t)+\mathcal{D}R_i(\mathcal{D})\hat{\sigma}(\varphi_M(t))=\Phi_0^{(C)},\\ \Phi_0^{(C)}\in\mathbb{R}.\end{cases} \tag{68}$$

Proof. The proof is similar to that of Proposition 2 once it is observed that, since $i_M=\mathcal{D}q_M=\mathcal{D}^2\sigma_M$, Eq. (67) can be equivalently rewritten as the following differential equation of order n_i+1

$$\begin{aligned}&P_i(\mathcal{D})\mathcal{D}\varphi_M(t)+R_i(\mathcal{D})\mathcal{D}q_M(t)\\ &\quad=\mathcal{D}(P_i(\mathcal{D})\varphi_M(t)+\mathcal{D}R_i(\mathcal{D})\sigma_M(t))=0,\end{aligned} \tag{69}$$

and that the degree of $\mathcal{D}R_i(\mathcal{D})$ is strictly less than that of $P_i(\mathcal{D})$. In particular, according to (30), it turns out that the scalar variable

$$\begin{aligned}\Phi^{(C)}(t)&\doteq P_i(\mathcal{D})\varphi_M(t)+\mathcal{D}R_i(\mathcal{D})\sigma_M(t)\\ &=P_i(\mathcal{D})\varphi_M(t)+\mathcal{D}R_i(\mathcal{D})\hat{\sigma}(\varphi_M(t))\end{aligned} \tag{70}$$

is constant over time, i.e.

$$\Phi^{(C)}(t)=\Phi^{(C)}(t_0)\doteq\Phi_0^{(C)}\quad\forall\,t\geq t_0, \tag{71}$$

where $\Phi_0^{(C)}$ is given by the sum of the initial conditions $\mathcal{D}^{n_i-1}v_M(t_0)$ and a term depending only on the remaining initial conditions $\varphi_M(t_0), v_M(t_0)$, $\mathcal{D}v_M(t_0),\ldots,\mathcal{D}^{n_v-2}v_M(t_0)$. ■

Remark 3.5. Note that also $\Sigma_{\Phi_0^{(C)}}$ admits a first integral and it is equivalently described by the

input–output relation

$$\varphi_M(t) = -\mathcal{D}L_i(\mathcal{D})\hat{\sigma}(\varphi_M(t)) + \frac{1}{P_v(\mathcal{D})}\Phi_0^{(C)}, \quad \Phi_0^{(C)} \in \mathbb{R}. \tag{72}$$

Hence, also $\Sigma_{\Phi_0^{(C)}}$ can be put in the form of Fig. 6 once

$$y = \varphi_M, \quad n(\cdot) = \hat{\sigma}(\cdot), \quad n(y) = \sigma_M,$$
$$L_1(\mathcal{D}) = \mathcal{D}L_i(\mathcal{D}), \quad L_2(\mathcal{D}) = \frac{1}{P_i(\mathcal{D})}, \quad r = \Phi_0^{(C)}. \tag{73}$$

Finally, note that Proposition 4 requires that the relative degree of $L_i(\mathcal{D})$ is greater than one and, hence, according to Remark 2.1, **L** must be an active two-terminal input. If the relative degree of $L_i(\mathcal{D})$ is equal to one, then a conclusion analogous to that of Remark 3.4 is reached, i.e. $\Sigma_{\Phi_0^{(C)}}$ does not provide an equivalent representation of (67) for all the nonlinear characteristics (30).

The observation of Remark 3.5 on the relative degree of $L_i(\mathcal{D})$ implies that $\mathbf{MC}_\varphi$ can be interconnected, among the two-terminal elements of Fig. 3, only with that of Fig. 3(d).

Consider now the class of circuits of Fig. 1 with $\mathbf{MC}_\sigma$ as **ME**. In this case, the dynamics of the relative representation of Fig. 5(b) obeys

$$\begin{cases} P_v(\mathcal{D})i_M(t) + R_v(\mathcal{D})v_M(t) = 0, \\ \mathcal{D}\sigma_M(t) = q_M(t), \\ \mathcal{D}q_M(t) = i_M(t), \end{cases} \tag{74}$$

where v_M is obtained from σ_M and q_M according to the third equation in (33). The next result holds true.

Proposition 5. *Consider the class of circuits of Fig. 1 with* $\mathbf{MC}_\sigma$ *as* **ME** *and* **L** *such that* $L_v(\mathcal{D})$ *is proper and let Assumption 2.1 hold. Then, the dynamics of the class of circuits is completely described by the one-parameter family of differential equations of order* $n_v + 1$

$$\Sigma_{Q_0^{(C)}}: \begin{cases} \mathcal{D}P_v(\mathcal{D})\sigma_M(t) + R_v(\mathcal{D})\hat{\varphi}(\sigma_M(t)) = Q_0^{(C)}, \\ Q_0^{(C)} \in \mathbb{R}. \end{cases} \tag{75}$$

Proof. The proof is similar to that of Proposition 2 once it is observed that (74) can be equivalently rewritten as a unique differential equation of order $n_v + 2$

$$P_v(\mathcal{D})\mathcal{D}^2\sigma_M(t) + R_v(\mathcal{D})\mathcal{D}\varphi_M(t) = \mathcal{D}(\mathcal{D}P_v(\mathcal{D})\sigma_M(t) + R_v(\mathcal{D})\varphi_M(t)) = 0 \tag{76}$$

and that the degree $R_v(\mathcal{D})$ is strictly less than that of $\mathcal{D}P_v(\mathcal{D})$. In particular, it turns out that the scalar variable

$$Q^{(C)}(t) \doteq \mathcal{D}P_v(\mathcal{D})\sigma_M(t) + R_v(\mathcal{D})\varphi_M(t) = \mathcal{D}P_v(\mathcal{D})\sigma_M(t) + R_v(\mathcal{D})\hat{\varphi}(\sigma_M(t)) \tag{77}$$

is constant over time, i.e.

$$Q^{(C)}(t) = Q^{(C)}(t_0) \doteq Q_0^{(C)} \quad \forall\, t \geq t_0, \tag{78}$$

where $Q_0^{(C)}$ is given by the sum of the initial conditions $\mathcal{D}^{n_v-1}i_M(t_0)$ and a term depending only on the remaining initial conditions $\sigma_M(t_0), q_M(t_0), i_M(t_0), \mathcal{D}i_M(t_0), \ldots, \mathcal{D}^{n_v-2}i_M(t_0)$. ■

Remark 3.6. Note that also $\Sigma_{Q_0^{(C)}}$ admits a first integral and it is equivalently described by the input–output relation

$$\sigma_M(t) = -\frac{1}{D}L_v(\mathcal{D})\hat{\varphi}(\varphi_M(t)) + \frac{1}{\mathcal{D}P_v(\mathcal{D})}Q_0^{(C)}, \quad Q_0^{(C)} \in \mathbb{R}. \tag{79}$$

Hence, $\Sigma_{Q_0^{(C)}}$ can be put in the form of Fig. 6 once

$$y = \sigma_M, \quad n(\cdot) = \hat{\varphi}(\cdot),$$
$$n(y) = \varphi_M, \quad L_1(\mathcal{D}) = \frac{1}{D}L_v(\mathcal{D}), \tag{80}$$
$$L_2(\mathcal{D}) = \frac{1}{\mathcal{D}P_v(\mathcal{D})}, \quad r = Q_0^{(C)}.$$

Proposition 5 implies that $\mathbf{MC}_\sigma$ can be interconnected, among the two-terminal elements of Fig. 3, with those of Figs. 3(b), 3(c) and 3(e).

3.3. *The case of ideal meminductor*

Consider now the class of circuits of Fig. 1 with $\mathbf{ML}_\rho$ as **ME**. In this case, the dynamics of the relative representation of Fig. 5(a) obeys

$$\begin{cases} P_i(\mathcal{D})v_M(t) + R_i(\mathcal{D})i_M(t) = 0, \\ \mathcal{D}\rho_M(t) = \varphi_M(t), \\ \mathcal{D}\varphi_M(t) = v_M(t), \end{cases} \tag{81}$$

where i_M is obtained from ρ_M and φ_M according to the third equation in (35). The next result holds true.

Proposition 6. *Consider the class of circuits of Fig. 1 with* $\mathbf{ML}_\rho$ *as* **ME** *and* **L** *such that* $L_i(\mathcal{D})$ *is proper and let Assumption 2.1 hold. Then, the dynamics of the class of circuits is completely described by the one-parameter family of differential equations of order* $n_i + 1$

$$\Sigma_{\Phi_0^{(L)}}: \begin{cases} \mathcal{D}P_i(\mathcal{D})\rho_M(t) + R_i(\mathcal{D})\hat{q}(\rho_M(t)) = \Phi_0^{(L)} \\ \Phi_0^{(L)} \in \mathbb{R}. \end{cases} \tag{82}$$

Proof. The proof parallels that of Proposition 5 once v_M, i_M, φ_M, q_M, σ_M, $L_v(\mathcal{D})$ and $\hat{\varphi}(\cdot)$ are replaced with i_M, v_M, q_M, φ_M, ρ_M and $L_i(\mathcal{D})$ and $\hat{q}(\cdot)$, respectively. In particular, it turns out the scalar variable

$$\begin{aligned} \Phi^{(L)}(t) &\doteq \mathcal{D}P_i(\mathcal{D})\rho_M(t) + R_i(\mathcal{D})q_M(t) \\ &= \mathcal{D}P_i(\mathcal{D})\rho_M(t) + R_i(\mathcal{D})\hat{q}(\rho_M(t)) \end{aligned} \tag{83}$$

is constant over time, i.e.

$$\Phi^{(L)}(t) = \Phi^{(L)}(t_0) \doteq \Phi_0^{(L)} \quad \forall\, t \geq t_0, \tag{84}$$

where $\Phi_0^{(L)}$ is given by the sum of the initial conditions $\mathcal{D}^{n_i-1}v_M(t_0)$ and a term depending only on the remaining initial conditions $\rho_M(t_0), \varphi_M(t_0)$, $v_M(t_0), \mathcal{D}v_M(t_0), \ldots, \mathcal{D}^{n_v-2}v_M(t_0)$. ■

Remark 3.7. Note that also $\Sigma_{\Phi_0^{(L)}}$ admits a first integral and it is equivalently described by the input–output relation

$$\rho_M(t) = -\frac{1}{D}L_i(\mathcal{D})\hat{q}(\rho_M(t)) + \frac{1}{\mathcal{D}P_i(\mathcal{D})}\Phi_0^{(L)}, \quad \Phi_0^{(L)} \in \mathbb{R}. \tag{85}$$

Hence, $\Sigma_{\Phi_0^{(L)}}$ can be put in the form of Fig. 6 once

$$\begin{aligned} &y = \rho_M, \quad n(\cdot) = \hat{q}(\cdot), \\ &n(y) = q_M, \quad L_1(\mathcal{D}) = \frac{1}{D}L_i(\mathcal{D}), \\ &L_2(\mathcal{D}) = \frac{1}{\mathcal{D}P_i(\mathcal{D})}, \quad r = \Phi_0^{(L)}. \end{aligned} \tag{86}$$

Proposition 6 implies that $\mathbf{ML}_\rho$ can be interconnected, among the two-terminal elements of Fig. 3, with those of Figs. 3(a), 3(c) and 3(d).

Consider the class of circuits of Fig. 1 with $\mathbf{ML}_q$ as **ME**. In this case, the dynamics of the relative representation of Fig. 5(b) is governed by

$$\begin{cases} P_v(\mathcal{D})i_M(t) + R_v(\mathcal{D})v_M(t) = 0, \\ \mathcal{D}q_M(t) = i_M(t), \end{cases} \tag{87}$$

where v_M is obtained from φ_M and i_M according to the second and third equations in (37). We have the following result.

Proposition 7. *Consider the class of circuits of Fig. 1 with* $\mathbf{ML}_q$ *as* **ME** *and* **L** *such that* $L_v(\mathcal{D})$ *has relative degree greater than one, i.e.* $r_{n_v} = r_{n_v-1} = 0$, *and let Assumption 2.1 hold. Then, the dynamics of the class of circuits is completely described by the one-parameter family of differential equations of order* n_v

$$\Sigma_{Q_0^{(L)}}: \begin{cases} P_v(\mathcal{D})q_M(t) + \mathcal{D}R_v(\mathcal{D})\hat{\rho}(q_M(t)) = Q_0^{(L)}, \\ Q_0^{(L)} \in \mathbb{R}. \end{cases} \tag{88}$$

Proof. The proof parallels that of Proposition 4 once i_M, v_M, q_M, φ_M, σ_M, $L_i(\mathcal{D})$ and $\hat{\sigma}(\cdot)$ are replaced with v_M, i_M, φ_M, q_M, ρ_M and $L_v(\mathcal{D})$ and $\hat{\rho}(\cdot)$, respectively. In particular, it turns out that the scalar variable

$$\begin{aligned} Q^{(L)}(t) &\doteq P_v(\mathcal{D})q_M(t) + \mathcal{D}R_v(\mathcal{D})\rho_M(t) \\ &= P_v(\mathcal{D})q_M(t) + \mathcal{D}R_v(\mathcal{D})\hat{\rho}(q_M(t)) \end{aligned} \tag{89}$$

is constant over time, i.e.

$$Q^{(L)}(t) = Q^{(L)}(t_0) \doteq Q_0^{(L)} \quad \forall\, t \geq t_0, \tag{90}$$

where $Q_0^{(L)}$ is given by the sum of the initial conditions $\mathcal{D}^{n_v-1}i_M(t_0)$ and a term depending only on the remaining initial conditions $q_M(t_0), i_M(t_0)$, $\mathcal{D}i_M(t_0), \ldots, \mathcal{D}^{n_v-2}i_M(t_0)$. ■

Remark 3.8. Note that also $\Sigma_{Q_0^{(L)}}$ admits a first integral and it is equivalently described by the input–output relation

$$q_M(t) = -\mathcal{D}L_v(\mathcal{D})\hat{\rho}(q_M(t)) + \frac{1}{P_v(\mathcal{D})}Q_0^{(L)}, \quad Q_0^{(L)} \in \mathbb{R}. \tag{91}$$

Hence, $\Sigma_{Q_0^{(L)}}$ can be put in the form of Fig. 6 once

$$y = q_M, \quad n(\cdot) = \hat{\rho}(\cdot), \quad n(y) = \rho_M,$$

$$L_1(\mathcal{D}) = \mathcal{D}L_v(\mathcal{D}), \quad L_2(\mathcal{D}) = \frac{1}{P_v(\mathcal{D})}, \quad r = Q_0^{(L)}. \tag{92}$$

Finally, note that, if $L_v(\mathcal{D})$ has relative degree equal to one, then a conclusion analogous to that of Remark 3.4 is reached. Moreover, the condition of Proposition 7 on the relative degree of $L_v(\mathcal{D})$ requires that **L** must be an active two-terminal element.

The last observation of Remark 3.8 implies that $\mathbf{ML}_q$ can be interconnected, among the two-terminal elements of Fig. 3, only with that of Fig. 3(e).

3.4. *Summary of the results*

In the previous subsections it has been shown that each one of the six representations in the voltage–current domain can be equivalently described via the canonical input–output representation of Fig. 6, where the external input r is assumed to be any constant value. Table 1 summarizes the obtained results for each one of the representations. Specifically, for each memelement **ME** a column is reported containing the order of its dynamical model, the models $\mathcal{ML}$ and Σ and their relative orders, the output y, the nonlinearity $n(\cdot)$ and its output $n(y)$, the constant input r, the rational functions $L_1(\mathcal{D})$ and $L_2(\mathcal{D})$ together with the conditions on their coefficients. The table clearly highlights that, for each **ME**, the order of the system Σ is equal to that of the original representation in the voltage–current domain minus one, which is due to the fact that the dynamics of the original representation admits a first integral. Also, the input and output of the nonlinear subsystem are the flux φ_M and the charge q_M or their time integrals ρ_M and σ_M, which puts into evidence the importance of the flux-charge approach recently developed (see, e.g. [Corinto & Forti, 2016]) for the analysis of circuits containing memelements. Clearly, the voltage v_M and the current i_M of each memelement can be obtained by simply differentiating the input and the output of the nonlinear subsystem.

An application example is now developed to show how the canonical input–output representation can be readily obtained for a given circuit containing a memelement.

Example 3.4. Consider the celebrated Chua's circuit reported in Fig. 8(a) with the nonlinear resistor (Chua's diode) replaced by a memristor $\mathbf{MR}_\varphi$. It can be verified that the impedance of $L_i(\mathcal{D})$ of **L** is such that

$$L_i(\mathcal{D}) = \frac{\frac{1}{C_1}\left(\mathcal{D}^2 + \frac{1}{RC_2}\mathcal{D} + \frac{1}{LC_2}\right)}{\mathcal{D}^3 + \frac{C_1+C_2}{RC_1C_2}\mathcal{D}^2 + \frac{1}{LC_2}\mathcal{D} + \frac{1}{RLC_1C_2}} \tag{93}$$

and hence

$$P_i(\mathcal{D}) = \mathcal{D}^3 + \frac{C_1+C_2}{RC_1C_2}\mathcal{D}^2 + \frac{1}{LC_2}\mathcal{D} + \frac{1}{RLC_1C_2}. \tag{94}$$

Table 1. Summary of the characteristics of the canonical input–output representation related to each **ME**.

ME	$\mathbf{MR}_\varphi$	$\mathbf{MR}_q$	$\mathbf{MC}_\varphi$	$\mathbf{MC}_\sigma$	$\mathbf{ML}_\rho$	$\mathbf{ML}_q$
ME order	1	1	1	2	2	1
$\mathcal{ML}$	$\mathcal{ML}_{i,v}$	$\mathcal{ML}_{v,i}$	$\mathcal{ML}_{i,v}$	$\mathcal{ML}_{v,i}$	$\mathcal{ML}_{i,v}$	$\mathcal{ML}_{v,i}$
$\mathcal{ML}$ order	n_i	n_v	n_i	n_v	n_i	n_v
Σ	$\Sigma_{\Phi_0^{(R)}}$	$\Sigma_{Q_0^{(R)}}$	$\Sigma_{\Phi_0^{(C)}}$	$\Sigma_{Q_0^{(C)}}$	$\Sigma_{\Phi_0^{(L)}}$	$\Sigma_{Q_0^{(L)}}$
Σ order	n_i	n_v	n_i	n_v+1	n_i+1	n_v
y	φ_M	q_M	φ_M	σ_M	ρ_M	q_M
$n(\cdot)$	$\hat{q}(\cdot)$	$\hat{\varphi}(\cdot)$	$\hat{\sigma}(\cdot)$	$\hat{\varphi}(\cdot)$	$\hat{q}(\cdot)$	$\hat{\rho}(\cdot)$
$n(y)$	q_M	φ_M	σ_M	φ_M	q_M	ρ_M
r	$\Phi_0^{(R)}$	$Q_0^{(R)}$	$\Phi_0^{(C)}$	$Q_0^{(C)}$	$\Phi_0^{(L)}$	$Q_0^{(L)}$
$L_1(\mathcal{D})$	$L_i(\mathcal{D})$	$L_v(\mathcal{D})$	$\mathcal{D}L_i(\mathcal{D})$	$\frac{1}{\mathcal{D}}L_v(\mathcal{D})$	$\frac{1}{\mathcal{D}}L_i(\mathcal{D})$	$\mathcal{D}L_v(\mathcal{D})$
$L_2(\mathcal{D})$	$\frac{1}{P_i(\mathcal{D})}$	$\frac{1}{P_v(\mathcal{D})}$	$\frac{1}{P_i(\mathcal{D})}$	$\frac{1}{\mathcal{D}P_v(\mathcal{D})}$	$\frac{1}{\mathcal{D}P_i(\mathcal{D})}$	$\frac{1}{P_v(\mathcal{D})}$
Conditions	$r_{n_i}=0$	$r_{n_v}=0$	$r_{n_i}=r_{n_i-1}=0$			$r_{n_v}=r_{n_v-1}=0$

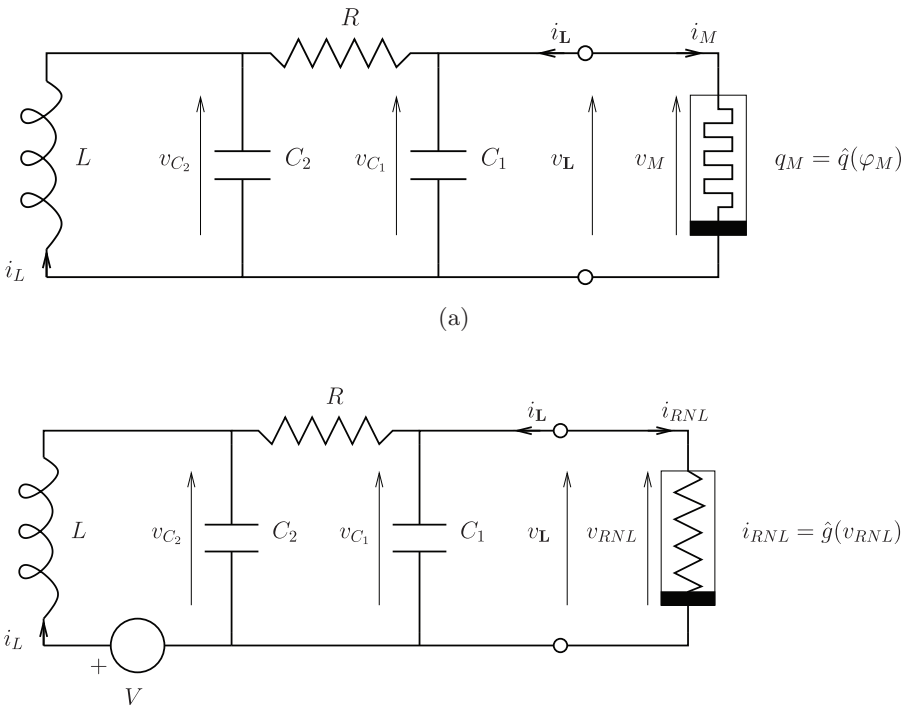

Fig. 8. (a) Memristive Chua's circuit and (b) equivalent circuit with the nonlinear resistor in place of the memristor and the additional constant voltage generator.

According to the first column of Table 1, the canonical input–output representation of the memristive Chua's circuit is in Fig. 9, with $L_i(\mathcal{D})$ and $P_i(\mathcal{D})$ as in (93) and (94), respectively, and

$$\Phi_0^{(R)} = \mathcal{D}^2 v_M(t_0) + \frac{C_1 + C_2}{RC_1C_2}\mathcal{D}v_M(t_0) + \frac{1}{LC_2}v_M(t_0) + \frac{1}{RLC_1C_2}\varphi_M(t_0)$$

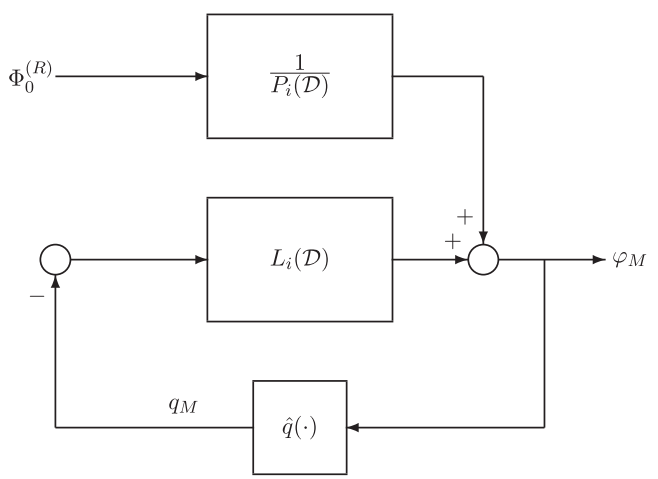

Fig. 9. The canonical input–output representation of the memristive Chua's circuit.

$$+ \frac{1}{C_1}\mathcal{D}^2\hat{q}(\varphi_M(t_0)) + \frac{1}{RCC_2}\mathcal{D}\hat{q}(\varphi_M(t_0)) + \frac{1}{LC_1C_2}\hat{q}(\varphi_M(t_0)). \quad (95)$$

The dynamics of the memristive Chua's circuit is thus obtained by collecting the dynamical behaviors of the canonical representation generated by all the constant values $\Phi_0^{(R)}$. It is interesting to note that the dynamical behaviors pertaining to a given value of $\Phi_0^{(R)}$ are exactly those displayed by the classical Chua's circuit of Fig. 8(b) where the memristor is replaced by a nonlinear resistor with voltage–current characteristic such that $\hat{g}(\cdot) = \hat{q}(\cdot)$, i.e. $i_{RNL} = \hat{q}(v_{RNL})$, forced by an additional constant voltage generator given by

$$V = \Phi_0^{(R)} RLC_1C_2. \quad (96)$$

Hence, the dynamics of the memristive Chua's circuit can be equivalently obtained via a family of classical Chua's circuit, which clearly highlights the richness of a memristive circuit over a classical one (see also [Di Marco *et al.*, 2018]).

Remark 3.9. It is worth underlining that having reduced the study of the dynamics of the class of

circuits in Fig. 1 to the analysis of a system enjoying the structure of Σ is quite important. Indeed, Σ is completely defined by the nonlinear characteristic pertaining to **ME** and the impedance or admittance of **L**. In this respect, note that the impedance and admittance can be obtained experimentally even if a model is not available. Moreover, several tools are available for the dynamical analysis of systems enjoying this structure, including the well-known Harmonic Balance Method (HBM) [Atherton, 1975; Mees, 1981; Khalil, 2002]. The HBM has been widely used to predict periodic solutions, their bifurcations and more complex dynamics [Genesio & Tesi, 1992; Piccardi, 1994; Tesi *et al.*, 1996; Basso *et al.*, 1997; Bonani & Gilli, 1999; Di Marco *et al.*, 2003; Innocenti *et al.*, 2010; Di Marco *et al.*, 2018; Innocenti *et al.*, 2019b]. In a forthcoming paper, it will be applied in a systematic way to the canonical input–output system Σ.

4. State Space Representations and Invariant Manifolds Characterization

In this section, we focus on state space representation of the six interconnected systems of Fig. 5. First, we introduce a suitable state representation of the current–voltage and the voltage–current models of **L**,[3] by considering that the input and the output of $\mathcal{ML}_{i,v}$ are $i_{\mathbf{L}}$ and $v_{\mathbf{L}}$ [see Fig. 5(a)], while those of $\mathcal{ML}_{v,i}$ are $-v_{\mathbf{L}}$ and $-i_{\mathbf{L}}$ [see Fig. 5(a)], respectively.

Proposition 8. *Let Assumption 2.1 hold and consider the state space representation*

$$\begin{cases} \mathcal{D}x(t) = Ax(t) + Bu(t), \\ z(t) = Cx(t) + Du(t), \end{cases} \tag{97}$$

where $x \in \mathbb{R}^N$ is the state vector, u is the scalar input, z is the scalar output, and $A \in \mathbb{R}^{N\times N}$, $B \in \mathbb{R}^{N\times 1}$, $C \in \mathbb{R}^{1\times N}$, $D \in \mathbb{R}^{1\times 1}$ are the following matrices:

$$A = \begin{pmatrix} -p_{N-1} & 1 & 0 & \cdots & 0 \\ -p_{N-2} & 0 & 1 & \cdots & 0 \\ \vdots & \vdots & \vdots & \ddots & \vdots \\ -p_1 & 0 & 0 & \cdots & 1 \\ -p_0 & 0 & 0 & \cdots & 0 \end{pmatrix},$$

$$B = \begin{pmatrix} r_{N-1} - r_N p_{N-1} \\ r_{N-2} - r_N p_{N-2} \\ \vdots \\ r_1 - r_N p_1 \\ r_0 - r_N p_0 \end{pmatrix},$$

$$C = (1 \quad 0 \quad \cdots \quad 0 \quad 0),$$

$$D = r_N. \tag{98}$$

Then, $\mathcal{ML}_{i,v}$ and $\mathcal{ML}_{v,i}$ admit the state representations (97)–(98) with $N = n_i$, $u = i_{\mathbf{L}}$, $z = v_{\mathbf{L}}$ and $N = n_v$, $u = -v_{\mathbf{L}}$, $z = -i_{\mathbf{L}}$, respectively.

Proof. The proof follows from Assumption 2.1 and by observing that in the $\mathcal{ML}_{i,v}$ case[4]

$$C(\mathcal{D}I_N - A)^{-1}B + D = L_i(\mathcal{D}) \tag{99}$$

and in the $\mathcal{ML}_{v,i}$ case

$$C(\mathcal{D}I_N - A)^{-1}B + D = L_v(\mathcal{D}). \tag{100}$$

■

Remark 4.1. Note that if $L_i(\mathcal{D})$ and $L_v(\mathcal{D})$ are strictly proper, i.e. $r_{n_i} = r_{n_v} = 0$, then $D = 0$ and $B = (r_{N-1}, r_{N-2}, \ldots, r_1, r_0)^\top$. Moreover, if $L_i(\mathcal{D})$ and $L_v(\mathcal{D})$ have relative degree greater than one, i.e. $r_{n_i} = r_{n_i-1} = r_{n_v} = r_{n_v-1} = 0$, then $D = 0$ and $B = (0, r_{N-2}, \ldots, r_1, r_0)^\top$.

Remark 4.2. There are infinite equivalent state space representations depending on the choice of the state vector x. For instance, consider the natural representation in the voltage–current domain where the state vector $\overline{x} \in \mathbb{R}^N$ collects the voltages of all capacitors and the currents of all inductors of **L**. Let us write this new state representation as

$$\begin{cases} \mathcal{D}\overline{x}(t) = \overline{A}\overline{x}(t) + \overline{B}u(t), \\ z(t) = \overline{C}\overline{x}(t) + \overline{D}u(t), \end{cases} \tag{101}$$

where $\overline{A} \in \mathbb{R}^{N\times N}$, $\overline{B} \in \mathbb{R}^{N\times 1}$, $\overline{C} \in \mathbb{R}^{1\times N}$, $\overline{D} \in \mathbb{R}^{1\times 1}$, and $u = i_{\mathbf{L}}$, $z = v_{\mathbf{L}}$ in the $\mathcal{ML}_{i,v}$ case, while $u = -v_{\mathbf{L}}$, $z = -i_{\mathbf{L}}$ in the $\mathcal{ML}_{v,i}$ case. The unique nonsingular transformation matrix $S \in \mathbb{R}^{N\times N}$ such that $\overline{x} = S^{-1}x$ can be computed by solving the

[3]To avoid the trivial case we assume that the order N of **L**, defined as in Proposition 8, is such that $N > 1$. If $N = 1$ state space models boil down to the differential Eqs. (8) and (9).

[4]I_N denotes the identity matrix of order N.

linear equations

$$S\overline{A} = AS, \quad S\overline{B} = B, \quad \overline{C} = CS, \quad \overline{D} = D. \tag{102}$$

Let us now develop a state space representation of each one of the six systems of Fig. 5. The next result readily follows from Proposition 8 and Eqs. (27) and (29) describing the dynamics of $\mathbf{MR}_\varphi$ and $\mathbf{MR}_q$, respectively.

Proposition 9. *Let Assumption 2.1 hold and let $L_i(\mathcal{D})$ and $L_v(\mathcal{D})$ be strictly proper, i.e. $r_{n_i} = r_{n_v} = 0$, respectively. Then, the representation of Fig. 5(a) with $\mathbf{MR}_\varphi$ and the representation of Fig. 5(b) with $\mathbf{MR}_q$ admit the state space representation*

$$\mathcal{S}^{(I)}: \begin{pmatrix} \mathcal{D}\xi_1(t) \\ \mathcal{D}x(t) \end{pmatrix} = \begin{pmatrix} 0 & C \\ 0_{N\times 1} & A \end{pmatrix} \begin{pmatrix} \xi_1(t) \\ x(t) \end{pmatrix} - \begin{pmatrix} 0 \\ B \end{pmatrix} f'(\xi_1(t)) Cx(t), \tag{103}$$

once $N = n_i$, $\xi_1 = \varphi_M$, $f = \hat{q}$, and $N = n_v$, $\xi_1 = q_M$, $f = \hat{\varphi}$, respectively.

We can now show that (103) enjoys the fundamental property that its state space is foliated, i.e. it amounts to a continuum of invariant manifolds where different lower-order dynamical behaviors are displayed.

Proposition 10. *Let $(\xi_1(t), x(t))^\top \in \mathbb{R}^{N+1}$ be the solution for $t \geq t_0$ of the state representation $\mathcal{S}^{(I)}$ with initial condition $(\xi_1(t_0), x(t_0))^\top \in \mathbb{R}^{N+1}$. Then,*

$$(\xi_1(t), x(t))^\top \in \mathcal{M}_0^{(I)}, \quad \forall\, t \geq t_0, \tag{104}$$

where

$$\begin{aligned} \mathcal{M}_0^{(I)} = \{(\xi_1, x)^\top \in \mathbb{R}^{N+1} : {} & x_N + p_0\xi_1 + r_0 f(\xi_1) \\ & = x_N(t_0) + p_0\xi_1(t_0) + r_0 f(\xi_1(t_0)) \\ & \doteq K_0^{(I)}\}. \end{aligned} \tag{105}$$

The dynamics on the invariant manifold $\mathcal{M}_0^{(I)}$ is described by the equations

$$\begin{cases} \xi_1(t) = \eta_1(t), \\ x_i(t) = \eta_{i+1}(t) - p_{N-i}\eta_1(t) \\ \qquad\quad - r_{N-i} f(\eta_1(t)), \quad i = 1, \ldots, N-1, \\ x_N(t) = K_0^{(I)} - p_0\eta_1(t) - r_0 f(\eta_1(t)), \end{cases} \tag{106}$$

where $\eta(t) \in \mathbb{R}^N$ is the solution of the reduced order state space model

$$\mathcal{S}_R^{(I)}: \begin{pmatrix} \mathcal{D}\eta_1(t) \\ \mathcal{D}\eta_2(t) \\ \vdots \\ \mathcal{D}\eta_{N-1}(t) \\ \mathcal{D}\eta_N(t) \end{pmatrix} = A \begin{pmatrix} \eta_1(t) \\ \eta_2(t) \\ \vdots \\ \eta_{N-1}(t) \\ \eta_N(t) \end{pmatrix} - Bf(\eta_1(t)) + \begin{pmatrix} 0 \\ 0 \\ \vdots \\ 0 \\ K_0^{(I)} \end{pmatrix}, \tag{107}$$

with initial condition

$$\begin{aligned} (\xi_1(t_0), x_1(t_0) + p_{N-1}\xi_1(t_0) + r_{N-1} f(\xi_1(t_0)), \ldots, \\ x_{N-1}(t_0) + p_1\xi_1(t_0) + r_1 f(\xi_1(t_0)))^\top \in \mathbb{R}^N. \end{aligned}$$

Proof. See the Appendix. ■

Remark 4.3. Proposition 10 characterizes the invariant manifolds of the state space of the representation of Fig. 5(a) with $\mathbf{MR}_\varphi$, once $N = n_i$, $\xi_1 = \varphi_M$, $f = \hat{q}$, and that of Fig. 5(b) with $\mathbf{MR}_q$, once $N = n_v$, $\xi_1 = q_M$, $f = \hat{\varphi}$. In both cases any solution $(\xi_1(t), x(t))^\top$ of $\mathcal{S}^{(I)}$ can be computed by first obtaining $K_0^{(I)}$ according to the last equality in (105), then solving $\mathcal{S}_R^{(I)}$ for $\eta_1(t), \eta_2(t), \ldots, \eta_N(t)$ and finally using relations (106). In this respect, it is interesting to note that $\mathcal{S}_R^{(I)}$ does not contain the derivative of the function f, which is a useful property when piecewise linear flux-charge and charge-flux characteristics are considered.

Remark 4.4. Note that the solution $\eta_1(t)$ of (107) is such that

$$\eta_1(t) = -C(\mathcal{D}I_N - A)^{-1} Bf(\eta_1(t)) + \frac{K_0^{(I)}}{\det[\mathcal{D}I_N - A]}. \tag{108}$$

Hence, from Eqs. (99) and (100) and relations (48) and (54) it follows the constant $K_0^{(I)}$ is indeed equal to the parameter $\Phi_0^{(R)}$ defining the family $\Sigma_{\Phi_0^{(R)}}$, in the case of a flux-controlled memristor, while is

equal to the parameter $Q_0^{(R)}$ defining $\Sigma_{Q_0^{(R)}}$ in the charge-controlled case.

Remark 4.5. According to Remark 4.2, the invariant manifold $\mathcal{M}_0^{(I)}$ can be expressed in terms of the state vector $\overline{x}$ of (101) as

$$\sum_{h=1}^{N} s_{Nh}\overline{x}_h + p_0\xi_1 + r_0 f(\xi_1) = K_0^{(I)}, \quad (109)$$

where s_{Nh}, $h = 1, \ldots, N$ are the entries of the Nth row of S. It is interesting to note that the invariant manifold is linear when $r_0 = 0$, which means the polynomials $R_\varphi(\mathcal{D})$ and $R_q(\mathcal{D})$ must vanish at $\mathcal{D} = 0$.

Let us now develop a state space representation for the system of Fig. 5(a) with $\mathbf{MC}_\varphi$ and the one of Fig. 5(b) with $\mathbf{ML}_q$. The next result readily follows from Proposition 8 and relations (31), (37).

Proposition 11. *Let Assumption 2.1 hold and let $L_i(\mathcal{D})$ and $L_v(\mathcal{D})$ have relative degree less than one, i.e. $r_{n_i} = r_{n_i-1} = r_{n_v} = r_{n_v-1} = 0$. Then, the representation of Fig. 5(a) with $\mathbf{MC}_\varphi$ and the representation of Fig. 5(b) with $\mathbf{ML}_q$ admit the state space representation*

$$\mathcal{S}^{(II)}: \begin{pmatrix} \mathcal{D}\xi_1(t) \\ \mathcal{D}x(t) \end{pmatrix} = \begin{pmatrix} 0 & C \\ 0_{N\times 1} & A \end{pmatrix} \begin{pmatrix} \xi_1(t) \\ x(t) \end{pmatrix} - \begin{pmatrix} 0 \\ B \end{pmatrix} (f''(\xi_1(t))(Cx(t))^2 + f'(\xi_1(t))CAx(t)), \quad (110)$$

once $N = n_i$, $\xi_1 = \varphi_M$, $f = \hat{\sigma}$, and $N = n_v$, $\xi_1 = q_M$, $f = \hat{\rho}$, respectively.

It can be shown that also in this case the state space is foliated.

Proposition 12. *Let $(\xi_1(t), x(t))^\top \in \mathbb{R}^{N+1}$ be the solution for $t \geq t_0$ of $\mathcal{S}^{(II)}$ with initial condition $(\xi_1(t_0), x(t_0))^\top \in \mathbb{R}^{N+1}$. Then,*

$$(\xi_1(t), x(t))^\top \in \mathcal{M}_0^{(II)}, \quad \forall\, t \geq t_0, \quad (111)$$

where

$$\mathcal{M}_0^{(II)} = \{(\xi_1, x)^\top \in \mathbb{R}^{N+1} : x_N + p_0\xi_1 + r_0 f'(\xi_1)x_1 = x_N(t_0) + p_0\xi_1(t_0) + r_0 f'(\xi_1(t_0))x_1(t_0) \doteq K_0^{(II)}\}. \quad (112)$$

The dynamics on the invariant manifold $\mathcal{M}_0^{(II)}$ is described by the equations

$$\begin{cases} \xi_1(t) = \eta_1(t), \\ x_1(t) = \eta_2(t) - p_{N-1}\eta_1(t) - r_{N-2}f(\eta_1(t)), \\ x_i(t) = \eta_{i+1}(t) - p_{N-i}\eta_1(t) - r_{N-1-i}f(\eta_1(t)) \\ \qquad - r_{N-i}f'(\eta_1(t))(\eta_2(t) - p_{N-1}\eta_1(t) \\ \qquad - r_{N-2}f(\eta_1(t))), \quad i = 2, \ldots, N-1, \\ x_N(t) = K_0^{(II)} - p_0\eta_1(t) - r_0 f'(\eta_1(t))(\eta_2(t) \\ \qquad - p_{N-1}\eta_1(t) - r_{N-2}f(\eta_1(t))), \end{cases} \quad (113)$$

where $\eta(t) \in \mathbb{R}^N$ is the solution of the reduced order state space model

$$\mathcal{S}_R^{(II)}: \begin{pmatrix} \mathcal{D}\eta_1(t) \\ \mathcal{D}\eta_2(t) \\ \vdots \\ \mathcal{D}\eta_{N-1}(t) \\ \mathcal{D}\eta_N(t) \end{pmatrix} = A \begin{pmatrix} \eta_1(t) \\ \eta_2(t) \\ \vdots \\ \eta_{N-1}(t) \\ \eta_N(t) \end{pmatrix} - B_0 f(\eta_1(t)) + \begin{pmatrix} 0 \\ 0 \\ \vdots \\ 0 \\ K_0^{(II)} \end{pmatrix}, \quad (114)$$

with initial condition

$$(\xi_1(t_0), x_1(t_0) + p_{N-1}\xi_1(t_0) + r_{N-2}f(\xi_1(t_0)), x_2(t_0) + p_{N-2}\xi_1(t_0) + r_{N-3}f(\xi_1(t_0)) + r_{N-2}f'(\xi_1(t_0))x_1(t_0), \ldots, x_{N-1}(t_0) + p_1\xi_1(t_0) + r_0 f(\xi_1(t_0)) + r_1 f'(\xi_1(t_0))x_1(t_0))^\top \in \mathbb{R}^N$$

and

$$B_0 = (r_{N-2}, r_{N-3}, \ldots, r_0, 0)^\top \in \mathbb{R}^{N\times 1}.$$

Proof. See the Appendix. ■

Remark 4.6. Proposition 12 characterizes the state space invariant manifolds of the representation of Fig. 5(a) with $\mathbf{MC}_\varphi$, once $N = n_i$, $\xi_1 = \varphi_M$, $f = \hat{\sigma}$, and that of Fig. 5(b) with $\mathbf{ML}_q$, once $N = n_v$, $\xi_1 = q_M$, $f = \hat{\rho}$. In particular, according to Remark 4.2, the invariant manifold $\mathcal{M}_0^{(II)}$ can be

expressed in the voltage–current domain as

$$\sum_{h=1}^{N} s_{Nh}\overline{x}_h + p_0\xi_1 + r_0 f'(\xi_1)\overline{C}\overline{x} = K_0^{(II)}, \quad (115)$$

where s_{Nh}, $h = 1, \ldots, N$ are the entries of the Nth row of S and $\overline{C}$ is the output matrix in (101). Also in this case for $r_0 = 0$ the invariant manifold is linear. Finally, it can be verified that the constant $K_0^{(II)}$ is equal to the parameter $\Phi_0^{(C)}$ defining the family $\Sigma_{\Phi_0^{(C)}}$, in the case of $\mathbf{MC}_\varphi$, and to the parameter $Q_0^{(L)}$ defining $\Sigma_{Q_0^{(L)}}$ in the case of $\mathbf{ML}_q$.

We now consider a state space model for the representation of Fig. 5(a) with $\mathbf{ML}_\rho$ and the one of Fig. 5(b) with $\mathbf{MC}_\sigma$. The next result readily follows from Proposition 8 and relations (35), (37).

Proposition 13. *Let Assumption 2.1 hold. Then, the representation of Fig. 5(a) with $\mathbf{ML}_\rho$ and the representation of Fig. 5(b) with $\mathbf{MC}_\sigma$ admit the state space representation*

$$\begin{aligned}\mathcal{S}^{(III)}: \begin{pmatrix}\mathcal{D}\xi_1(t)\\ \mathcal{D}\xi_2(t)\\ \mathcal{D}x(t)\end{pmatrix} &= \begin{pmatrix}0 & 1 & 0_{1\times N}\\ 0 & 0 & C\\ 0_{N\times 1} & 0_{N\times 1} & A\end{pmatrix}\begin{pmatrix}\xi_1(t)\\ \xi_2(t)\\ x(t)\end{pmatrix}\\ &\quad - \begin{pmatrix}0\\ D\\ B\end{pmatrix} f'(\xi_1(t))\xi_2(t), \end{aligned} \quad (116)$$

once $N = n_i$, $\xi_1 = \rho_M$, $\xi_2 = \varphi_M$, $f = \hat{q}$, and $N = n_v$, $\xi_1 = \sigma_M$, $\xi_2 = q_M$, $f = \hat{\varphi}$, respectively.

It can be shown that also in this case the state space is foliated.

Proposition 14. *Let $(\xi_1(t), \xi_2(t), x(t))^\top \in \mathbb{R}^{N+2}$ be the solution for $t \geq t_0$ of $\mathcal{S}^{(II)}$ with initial condition $(\xi_1(t_0), \xi_2(t_0), x(t_0))^\top \in \mathbb{R}^{N+2}$. Then,*

$$(\xi_1(t), \xi_2(t), x(t))^\top \in \mathcal{M}_0^{(III)}, \quad \forall\, t \geq t_0, \quad (117)$$

where

$$\begin{aligned}\mathcal{M}_0^{(III)} = \{(\xi_1, \xi_2, x)^\top \in \mathbb{R}^{N+2} : x_N + p_0\xi_2 + r_0 f(\xi_1)\\ = x_N(t_0) + p_0\xi_2(t_0) + r_0 f(\xi_1(t_0))\\ \doteq K_0^{(III)}\}. \end{aligned} \quad (118)$$

The dynamics on the invariant manifold $\mathcal{M}_0^{(III)}$ is described by the equations

$$\begin{cases}\xi_1(t) = \eta_1(t),\\ \xi_2(t) = \eta_2(t) - p_{N-1}\eta_1(t) - r_N f(\eta_1(t)),\\ x_i(t) = \eta_{i+2}(t) - (p_{N-1-i} - p_{N-i}p_{N-1})\eta_1(t)\\ \qquad\quad - p_{N-i}\eta_2(t) - (r_{N-i} - p_{N-i}r_N)f(\eta_1(t)),\\ \qquad\qquad\qquad\qquad i = 2, \ldots, N-1,\\ x_N(t) = K_0^{(III)} + p_0 p_{N-1}\eta_1(t) - p_0\eta_2(t)\\ \qquad\quad - (r_0 - p_0 r_N)f(\eta_1(t)),\end{cases} \quad (119)$$

where $\eta(t) \in \mathbb{R}^{N+1}$ is the solution of the reduced order state space model

$$\begin{aligned}\mathcal{S}_R^{(III)}: \begin{pmatrix}\mathcal{D}\eta_1(t)\\ \mathcal{D}\eta_2(t)\\ \vdots\\ \mathcal{D}\eta_N(t)\\ \mathcal{D}\eta_{N+1}(t)\end{pmatrix} &= \begin{pmatrix}A & 0_{1\times N}\\ 0_{N\times 1} & 0\end{pmatrix}\begin{pmatrix}\eta_1(t)\\ \eta_2(t)\\ \vdots\\ \eta_N(t)\\ \eta_{N+1}(t)\end{pmatrix}\\ &\quad - \begin{pmatrix}D\\ B\end{pmatrix} f(\eta_1(t)) + \begin{pmatrix}0\\ 0\\ \vdots\\ 0\\ K_0^{(III)}\end{pmatrix}, \end{aligned} \quad (120)$$

with initial condition

$$\begin{aligned}(\xi_1(t_0), p_{N-1}\xi_1(t_0) + \xi_2(t_0) + r_N f(\xi_1(t_0)), x_1(t_0)\\ + p_{N-2}\xi_1(t_0) + p_{N-1}\xi_2(t_0)\\ + r_{N-1}f(\xi_1(t_0)), \ldots, x_{N-1}(t_0) + p_0\xi_1(t_0)\\ + p_1\xi_2(t_0) + r_1 f(\xi_1(t_0)))^\top \in \mathbb{R}^{N+1}.\end{aligned}$$

Proof. See the Appendix. ■

Remark 4.7. Proposition 14 characterizes the state space invariant manifolds of the representation of

Fig. 5(a) with $\mathbf{ML}_\rho$, once $N = n_i$, $\xi_1 = \rho_M$, $\xi_2 = \varphi_M$, $f = \hat{q}$, and that of Fig. 5(b) with $\mathbf{MC}_\sigma$, once $N = n_v$, $\xi_1 = \sigma_M$, $\xi_2 = q_M$, $f = \hat{\varphi}$. In particular, according to Remark 4.2, the invariant manifold $\mathcal{M}_0^{(III)}$ can be expressed in the voltage–current domain as

$$\sum_{h=1}^{N} s_{Nh}\overline{x}_h + p_0\xi_2 + r_0 f(\xi_1) = K_0^{(III)}, \qquad (121)$$

where s_{Nh}, $i = h, \ldots, N$ are the entries of the Nth row of S. Also in this case for $r_0 = 0$ the invariant manifold is linear. Finally, it can be verified that the constant $K_0^{(III)}$ is equal to the parameter $\Phi_0^{(L)}$ defining the family $\Sigma_{\Phi_0^{(L)}}$, in the case of $\mathbf{ML}_\rho$, and to the parameter $Q_0^{(C)}$ defining $\Sigma_{Q_0^{(C)}}$ in the case of $\mathbf{MC}_\sigma$.

Table 2 summarizes the expressions in the voltage–current domain of the invariant manifolds for each one of the six representations of Fig. 5. Specifically, $\overline{x} \in \mathbb{R}^N$ is the natural state vector in the voltage–current domain (see Remark 4.2) and s_{Nh} are the components of the last row of the matrix $S \in \mathbb{R}^{N\times N}$ which can be computed according to relations (102). The next example shows in some detail how to compute the invariant manifolds for all admissible interconnection between the two-terminal elements **L** of Fig. 3 and each **ME**.

Example 4.1. For the two-terminal element **L** of Fig. 3(a) the state vector in the voltage–current domain is $\overline{x} = (v_C, i_L)^\top \in \mathbb{R}^2$. It can be verified that its time evolution is described by the state space representation (101), where $u = i_{\mathbf{L}}$, $z = v_{\mathbf{L}}$ and

$$\overline{A} = \begin{pmatrix} 0 & \dfrac{1}{C} \\ -\dfrac{1}{L} & -\dfrac{R}{L} \end{pmatrix}, \quad \overline{B} = \begin{pmatrix} \dfrac{1}{C} \\ 0 \end{pmatrix}, \quad \overline{C} = (1 \quad 0), \quad \overline{D} = 0. \qquad (122)$$

From the expression of $L_i(\mathcal{D})$ in (12), we have $r_0 = R/(LC)$, $r_1 = 1/C$, $p_0 = 1/(LC)$, $p_1 = R/L$ and thus we get the matrices (98). To obtain the expressions in Table 2 of the invariant manifolds it remains to compute the last row of the matrix $S \in \mathbb{R}^{2\times 2}$. By solving the linear equations (102), we get $s_{21} = R/L$ and $s_{22} = 1/C$ and, hence, the analytical expressions of the invariant manifolds of the circuit of Fig. 3(a) with $\mathbf{MR}_\varphi$ and $\mathbf{ML}_\rho$ as **ME** are readily obtained (see Table 3).

Consider now the two-terminal element **L** of Fig. 3(b). The time evolution of the state vector

Table 2. Summary of the invariant manifolds of the state space representation related to each **ME**.

ME	Invariant Manifolds
$\mathbf{MR}_\varphi$	$\left\{(\varphi_M, \overline{x})^\top \in \mathbb{R}^{n_i+1} : \sum_{h=1}^{n_i} s_{n_i h}\overline{x}_h + p_0\varphi_M + r_0\hat{q}(\varphi_M) = \Phi_0^{(R)}, \Phi_0^{(R)} \in \mathbb{R}\right\}$
$\mathbf{MR}_q$	$\left\{(q_M, \overline{x})^\top \in \mathbb{R}^{n_v+1} : \sum_{h=1}^{n_v} s_{n_v h}\overline{x}_h + p_0 q_M + r_0\hat{\varphi}(q_M) = Q_0^{(R)}, Q_0^{(R)} \in \mathbb{R}\right\}$
$\mathbf{MC}_\varphi$	$\left\{(\varphi_M, \overline{x})^\top \in \mathbb{R}^{n_i+1} : \sum_{h=1}^{n_i} s_{n_i h}\overline{x}_h + p_0\varphi_M + r_0\hat{\sigma}'(\varphi_M)\overline{C}\overline{x} = \Phi_0^{(C)}, \Phi_0^{(C)} \in \mathbb{R}\right\}$
$\mathbf{MC}_\sigma$	$\left\{(\sigma_M, q_M, \overline{x})^\top \in \mathbb{R}^{n_v+2} : \sum_{h=1}^{n_v} s_{n_v h}\overline{x}_h + p_0 q_M + r_0\hat{\varphi}(\sigma_M) = Q_0^{(C)}, Q_0^{(C)} \in \mathbb{R}\right\}$
$\mathbf{ML}_\rho$	$\left\{(\rho_M, \varphi_M, \overline{x})^\top \in \mathbb{R}^{n_i+2} : \sum_{h=1}^{n_i} s_{n_i h}\overline{x}_h + p_0\varphi_M + r_0\hat{q}(\rho_M) = \Phi_0^{(L)}, \Phi_0^{(L)} \in \mathbb{R}\right\}$
$\mathbf{ML}_q$	$\left\{(q_M, \overline{x})^\top \in \mathbb{R}^{n_v+1} : \sum_{h=1}^{n_v} s_{n_v h}\overline{x}_h + p_0 q_M + r_0\hat{\rho}'(q_M)\overline{C}\overline{x} = Q_0^{(L)}, Q_0^{(L)} \in \mathbb{R}\right\}$

$\overline{x} = (v_C, i_L)^\top \in \mathbb{R}^2$ is described by the state space representation (101) where $u = -v_{\mathbf{L}}$, $z = -i_{\mathbf{L}}$ and

$$\overline{A} = \begin{pmatrix} 0 & \dfrac{1}{C} \\ -\dfrac{1}{L} & -\dfrac{R}{L} \end{pmatrix}, \quad \overline{B} = \begin{pmatrix} 0 \\ \dfrac{1}{L} \end{pmatrix}, \qquad (123)$$

$$\overline{C} = (0 \quad 1), \quad \overline{D} = 0.$$

From the expression of $L_v(\mathcal{D})$ in (12), it follows that $r_0 = 0$, $r_1 = 1/L$, $p_0 = 1/(LC)$, $p_1 = R/L$ from which we get the matrices (98). By solving (102), we obtain $s_{21} = 1/L$ and $s_{22} = 0$ which complete the analytical expression of the invariant manifolds of the circuit of Fig. 3(b) with $\mathbf{MR}_q$ and $\mathbf{MC}_\sigma$ as **ME** (see Table 3). It is interesting to note that, in this case, according to Remark 4.5, the invariant manifolds are linear.

Similar arguments apply to the linear two-terminal elements of Figs. 3(c)–3(e). The resulting invariant manifolds are reported in Table 3.

Two numerical examples are now developed to provide some insights on the structure of the invariant manifolds.

Example 4.2. Let us consider the interconnection between the passive circuit of Fig. 3(b) (with $R = 0.6$, $C = 0.5$ and $L = 1$) and a charge-controlled memristor $\mathbf{MR}_q$ with a cubic charge-flux characteristic given by

$$\varphi_M = \hat{\varphi}(q_M) = \alpha_0 q_M + \frac{\alpha_1}{3} q_M^3, \qquad (124)$$

Table 3. State space invariant manifolds of the admissible interconnection between the two-terminal elements **L** of Fig. 3 and each **ME**.

L	**ME**	Invariant Manifolds
Fig. 3(a)	$\mathbf{MR}_\varphi$	$\left\{(\varphi_M, v_C, i_L)^\top \in \mathbb{R}^3 : \frac{R}{L} v_C + \frac{1}{C} i_L + \frac{1}{LC}\varphi_M + \frac{R}{LC}\hat{q}(\varphi_M) = \Phi_0^{(R)}\right\}$
Fig. 3(a)	$\mathbf{ML}_\rho$	$\left\{(\rho_M, \varphi_M, v_C, i_L)^\top \in \mathbb{R}^4 : \frac{R}{L} v_C + \frac{1}{C} i_L + \frac{1}{LC}\varphi_M + \frac{R}{LC}\hat{q}(\rho_M) = \Phi_0^{(L)}\right\}$
Fig. 3(b)	$\mathbf{MR}_q$	$\left\{(q_M, v_C, i_L)^\top \in \mathbb{R}^3 : \frac{1}{L} v_C + \frac{1}{LC} q_M = Q_0^{(R)}\right\}$
Fig. 3(b)	$\mathbf{MC}_\sigma$	$\left\{(\sigma_M, q_M, v_C, i_L)^\top \in \mathbb{R}^4 : \frac{1}{L} v_C + \frac{1}{LC} q_M = Q_0^{(C)}\right\}$
Fig. 3(c)	$\mathbf{MC}_\sigma$	$\left\{(\sigma_M, q_M, v_C, i_L)^\top \in \mathbb{R}^4 : \frac{1}{L} v_C + \frac{1}{LC} q_M + \frac{1}{R_i LC}\hat{\varphi}(\sigma_M) = Q_0^{(C)}\right\}$
Fig. 3(c)	$\mathbf{ML}_\rho$	$\left\{(\rho_M, \varphi_M, v_C, i_L)^\top \in \mathbb{R}^4 : \frac{R_i}{L} v_C + \frac{1}{LC}\varphi_M + \frac{R_i}{LC}\hat{q}(\rho_M) = \Phi_0^{(L)}\right\}$
Fig. 3(d)	$\mathbf{MR}_\varphi$	$\left\{(\varphi_M, v_{C_1}, v_{C_2})^\top \in \mathbb{R}^3 : -\frac{1}{R_1 C_2} v_{C_1} + \frac{R_1 + R_2 + R_i}{R_1 R_i C_1} v_{C_2} + \frac{1}{R_1 R_i C_1 C_2}\left(\varphi_M + R_2 \hat{q}(\varphi_M)\right) = \Phi_0^{(R)}\right\}$
Fig. 3(d)	$\mathbf{MC}_\varphi$	$\left\{(\varphi_M, v_{C_1}, v_{C_2})^\top \in \mathbb{R}^3 : -\frac{1}{R_1 C_2} v_{C_1} + \frac{R_1 + R_2 + R_i}{R_1 R_i C_1} v_{C_2} + \frac{1}{R_1 R_i C_1 C_2}\left(\varphi_M + R_2 \hat{\sigma}'(\varphi_M) v_{C_2}\right) = \Phi_0^{(C)}\right\}$
Fig. 3(d)	$\mathbf{ML}_\rho$	$\left\{(\rho_M, \varphi_M, v_{C_1}, v_{C_2})^\top \in \mathbb{R}^4 : -\frac{1}{R_1 C_2} v_{C_1} + \frac{R_1 + R_2 + R_i}{R_1 R_i C_1} v_{C_2} + \frac{1}{R_1 R_i C_1 C_2}\left(\varphi_M + R_2 \hat{q}(\rho_M)\right) = \Phi_0^{(L)}\right\}$
Fig. 3(e)	$\mathbf{MR}_q$	$\left\{(q_M, v_{C_1}, v_{C_2})^\top \in \mathbb{R}^3 : \frac{-1}{R_1 R_3}\left(\frac{1}{C_2} v_{C_1} + \frac{1}{C_1} v_{C_2} - \frac{R_2 + R_3 + R_4}{R_2 C_1 C_2} q_M - \frac{1}{R_2 C_1 C_2}\hat{\varphi}(q_M)\right) = Q_0^{(R)}\right\}$
Fig. 3(e)	$\mathbf{MC}_\sigma$	$\left\{(\sigma_M, q_M, v_{C_1}, v_{C_2})^\top \in \mathbb{R}^4 : \frac{-1}{R_1 R_3}\left(\frac{1}{C_2} v_{C_1} + \frac{1}{C_1} v_{C_2} - \frac{R_2 + R_3 + R_4}{R_2 C_1 C_2} q_M - \frac{1}{R_2 C_1 C_2}\hat{\varphi}(\sigma_M)\right) = Q_0^{(C)}\right\}$
Fig. 3(e)	$\mathbf{ML}_q$	$\left\{(q_M, v_{C_1}, v_{C_2})^\top \in \mathbb{R}^3 : \frac{-1}{R_1 R_3}\left(\frac{1}{C_2} v_{C_1} + \frac{1}{C_1} v_{C_2} - \frac{R_2 + R_3 + R_4}{R_2 C_1 C_2} q_M + \frac{1}{R_2 R_3 C_1 C_2}\hat{\rho}'(q_M) v_{C_1}\right) = Q_0^{(R)}\right\}$

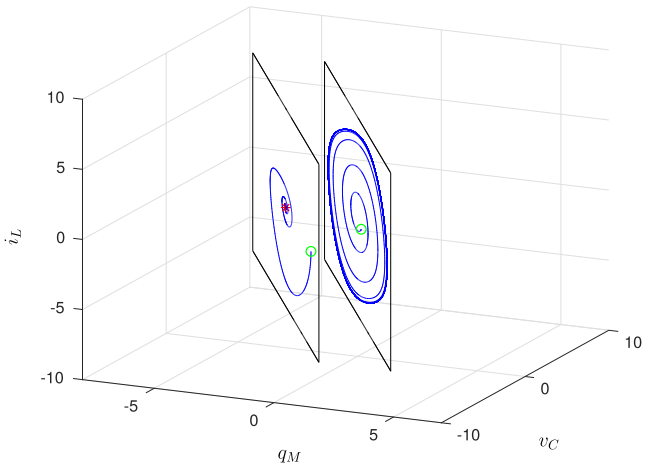

Fig. 10. Planar invariant manifolds (for $Q_0^{(R)} = -6$ and $Q_0^{(R)} = 0$) and state trajectories for the circuit obtained connecting the passive circuit of Fig. 3(b) with a charge-controlled memristor (Example 4.2). Initial conditions are marked with a green ∘ symbol, while stable equilibrium points are marked with a red ∗ symbol.

where $\alpha_0 = -1.02$ and $\alpha_1 = 0.1$. According to Table 3, the state space solutions $(q_M(t), v_C(t), i_L(t))$ evolve on planar manifolds. This property is highlighted by the trajectories illustrated in Fig. 10, which have initial conditions $(q_M(0) = 0.5, i_L(0) = -0.5, v_C(0) = -7)$ and $(q_M(0) = 0.5, i_L(0) = -0.5, v_C(0) = -1)$. They correspond to $Q_0^{(R)} = -6$ and $Q_0^{(R)} = 0$, respectively, and, therefore, evolve on different planar manifolds parallel to the i_L axis, as emphasized in the figure. Figure 11 shows the limit sets for several solutions of the circuit with initial conditions belonging to different invariant

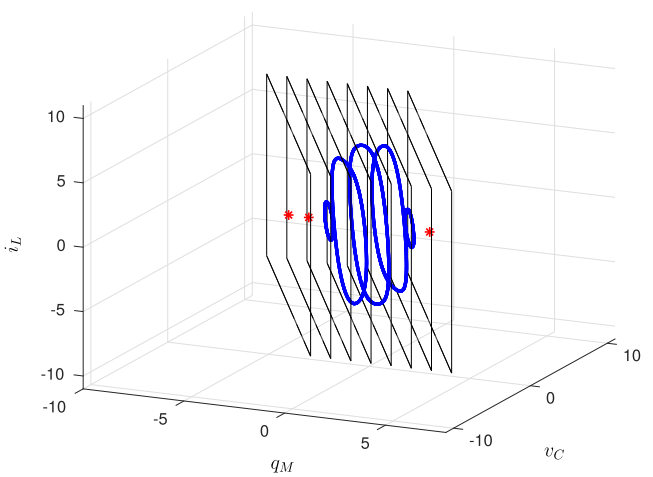

Fig. 11. Limit sets and planar invariant manifolds (for values of $Q_0^{(R)}$ between -8 and 6) for Example 4.2. Stable equilibrium points are marked with a red ∗ symbol.

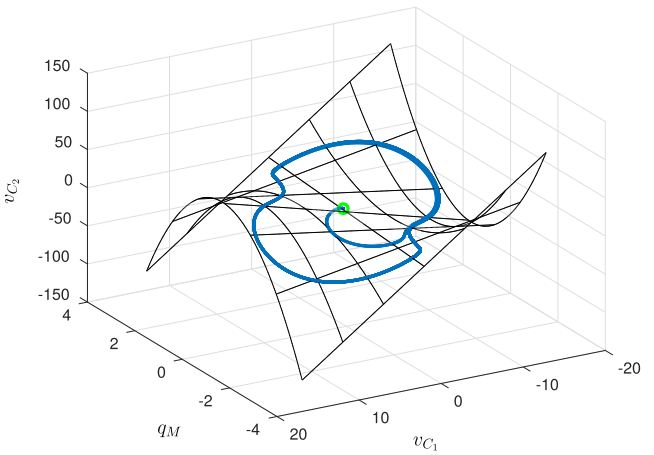

Fig. 12. Limit sets and nonplanar invariant manifold (corresponding to $Q_0^{(R)} = 0$) for Example 4.3. Initial conditions are marked with a green ∘ symbol.

manifolds. It can be noted that, depending on the initial conditions, the circuit shows both stationary and oscillatory solutions, thus it undergoes the so-called Hopf bifurcation "without parameters" [Fiedler *et al.*, 2000].

Example 4.3. Let us consider the interconnection between the active circuit of Fig. 3(e) (with $R_1 = 0.6$, $R_2 = 1$, $R_3 = 0.5$, $R_4 = 0.3$, $C_1 = 1$ and $C_2 = 0.6$) and a charge-controlled meminductor $\mathbf{ML}_q$ with a cubic charge-flux momentum characteristic given by

$$\rho_M = \hat{\rho}(q_M) = \alpha_0 q_M + \frac{\alpha_1}{3} q_M^3, \qquad (125)$$

where $\alpha_0 = -1.02$ and $\alpha_1 = 0.1$. Figure 12 shows the state evolution starting from initial conditions

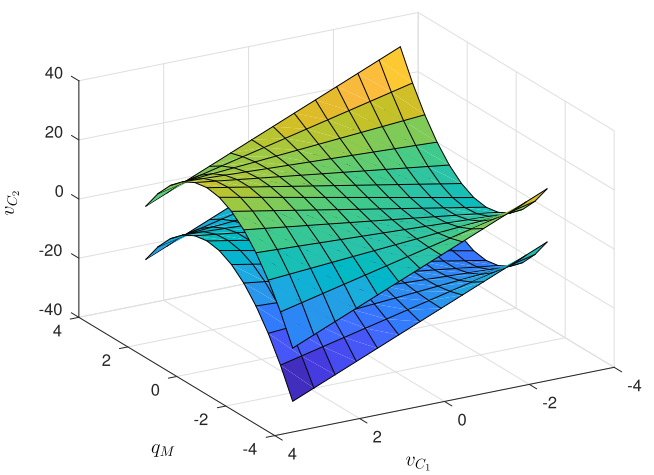

Fig. 13. Nonplanar invariant manifolds corresponding to $Q_0^{(R)} = -15$ and $Q_0^{(R)} = 15$ for Example 4.3.

$q_M(0) = 0.2$, $v_{C_1}(0) = -0.2$, $v_{C_2}(0) = 0.028$ and the associated invariant manifold corresponding to $Q_0^{(R)} = 0$, whose expression is reported in the last line of Table 3. Figure 13 shows two of such invariant manifolds, corresponding to $Q_0^{(R)} = -15$ and $Q_0^{(R)} = 15$, respectively.

5. Extension to the Case of Nonautonomous Classes of Circuits

In this section, we show how the structure of the canonical input–output system Σ of Fig. 6 can be suitably modified to incorporate also the case where $\mathbf{L}$ contains voltage or current generators. For the sake of simplicity, the analysis is limited to the case of a single generator $w(t)$, but the extension to the case of more generators is straightforward and it will be illustrated by an example.

The current–voltage model $\mathcal{ML}_{i,v}$ and the voltage–current model $\mathcal{ML}_{v,i}$ are assumed to be described by the following input–output relation

$$v_{\mathbf{L}}(t) = L_i(\mathcal{D})i_{\mathbf{L}}(t) + \overline{L}_i(\mathcal{D})w(t) \qquad (126)$$

and

$$i_{\mathbf{L}}(t) = L_v(\mathcal{D})v_{\mathbf{L}}(t) + \overline{L}_v(\mathcal{D})w(t), \qquad (127)$$

respectively. The rational function $L_i(\mathcal{D})$ (resp., $L_v(\mathcal{D})$) is as in (2) [resp., (5)], while

$$\overline{L}_i(\mathcal{D}) = \frac{\overline{R}_i(\mathcal{D})}{P_i(\mathcal{D})}, \quad \overline{L}_v(\mathcal{D}) = \frac{\overline{R}_v(\mathcal{D})}{P_v(\mathcal{D})} \qquad (128)$$

with $P_i(\mathcal{D})$ (resp., $P_v(\mathcal{D})$) as in (3) [resp., (6)] and

$$\overline{R}_i(\mathcal{D}) = \overline{r}_{n_i}\mathcal{D}^{n_i} + \overline{r}_{n_i-1}\mathcal{D}^{n_i-1} + \cdots + \overline{r}_1\mathcal{D} + \overline{r}_0,$$
$$\overline{R}_v(\mathcal{D}) = \overline{r}_{n_v}\mathcal{D}^{n_v} + \overline{r}_{n_v-1}\mathcal{D}^{n_v-1} + \cdots + \overline{r}_1\mathcal{D} + \overline{r}_0. \qquad (129)$$

The dynamics of $\mathcal{ML}_{i,v}$ is thus governed by the nonautonomous linear differential equation

$$P_i(\mathcal{D})v_{\mathbf{L}}(t) - R_i(\mathcal{D})i_{\mathbf{L}}(t) = \overline{R}_i(\mathcal{D})w(t), \qquad (130)$$

while that of $\mathcal{ML}_{v,i}$ by

$$P_v(\mathcal{D})i_{\mathbf{L}}(t) - R_v(\mathcal{D})v_{\mathbf{L}}(t) = \overline{R}_v(\mathcal{D})w(t). \qquad (131)$$

Let us now consider the six interconnections of Fig. 5 with $\mathcal{ML}_{i,v}$ and $\mathcal{ML}_{v,i}$ modeled by (130) and (131), respectively. Each one of these interconnections can be put in the form of the system Σ_F of Fig. 14, according to the next result.

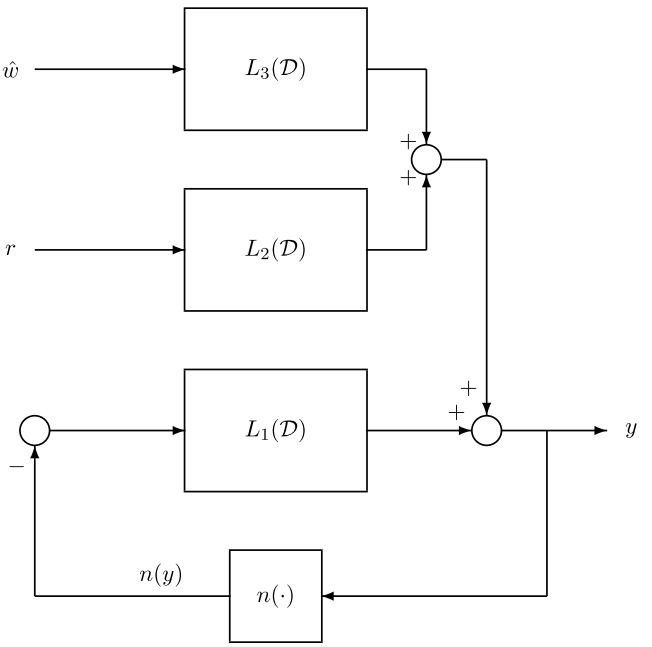

Fig. 14. System Σ_F: canonical input–output representation of the nonautonomous class of circuits.

Proposition 15. *The dynamics of the interconnections of $\mathcal{ML}_{i,v}$ in (130) with $\mathbf{MR}_\varphi$, $\mathbf{MC}_\varphi$, $\mathbf{ML}_\rho$, and of $\mathcal{ML}_{v,i}$ in (131) with $\mathbf{MR}_q$, $\mathbf{MC}_\sigma$, $\mathbf{ML}_q$ are described by the canonical system Σ_F where r is assumed to be any constant value (i.e. $r(t) = X_0$, $X_0 \in \mathbb{R}$), $\hat{w}$ is defined as*

$$\hat{w}(t) = \mathcal{D}^{-1}w(t) = \int_{-\infty}^{t} w(\sigma)d\sigma \qquad (132)$$

and for each memelement $L_1(\mathcal{D})$, $L_2(\mathcal{D})$, y, $n(\cdot)$, $n(y)$ are as in Table 1 and $L_3(\mathcal{D})$ is given in Table 4.

Proof. Let us focus on the interconnection between $\mathcal{ML}_{i,v}$ and $\mathbf{MR}_\varphi$. From (130) and (27) it can be

Table 4. Canonical system Σ_F: expression of the rational function $L_3(\mathcal{D})$ related to each **ME**.

ME	$L_3(\mathcal{D})$
$\mathbf{MR}_\varphi$	$\overline{L}_i(\mathcal{D})$
$\mathbf{MR}_q$	$\overline{L}_v(\mathcal{D})$
$\mathbf{MC}_\varphi$	$\overline{L}_i(\mathcal{D})$
$\mathbf{MC}_\sigma$	$\frac{1}{\mathcal{D}}\overline{L}_v(\mathcal{D})$
$\mathbf{ML}_\rho$	$\frac{1}{\mathcal{D}}\overline{L}_i(\mathcal{D})$
$\mathbf{ML}_q$	$\overline{L}_v(\mathcal{D})$

readily verified that the corresponding dynamics obeys

$$P_i(\mathcal{D})\mathcal{D}\varphi_M(t) + R_i(\mathcal{D})\mathcal{D}\hat{q}(\varphi_M(t)) = \overline{R}_i(\mathcal{D})w(t). \tag{133}$$

Now, since $w = \mathcal{D}\hat{w}$, (133) can be equivalently written as

$$\mathcal{D}(P_i(\mathcal{D})\varphi_M(t) + R_i(\mathcal{D})\hat{q}(\varphi_M(t)) - \overline{R}_i(\mathcal{D})\hat{w}(t)) = 0 \tag{134}$$

and hence the scalar variable

$$X(t) \doteq P_i(\mathcal{D})\varphi_M(t) + R_i(\mathcal{D})\hat{q}(\varphi_M(t)) - \overline{R}_i(\mathcal{D})\hat{w}(t) \tag{135}$$

is constant over time, i.e.

$$X(t) = X(t_0) \doteq X_0 \quad \forall\, t \geq t_0. \tag{136}$$

By reasoning as in the proof of Proposition 2, it can be shown that the family of reduced order nonautonomous differential equations

$$P_i(\mathcal{D})\varphi_M(t) + R_i(\mathcal{D})\hat{q}(\varphi_M(t)) = \overline{R}_i(\mathcal{D})\hat{w}(t) + X_0, \quad X_0 \in \mathbb{R} \tag{137}$$

generates all the solutions of the original differential equation (133). Clearly, the above family admits an equivalent representation in terms of the following input–output relation

$$\varphi_M(t) = -L_i(\mathcal{D})\hat{q}(\varphi_M(t)) + \overline{L}_i(\mathcal{D})\hat{w}(t) + \frac{1}{P_i(\mathcal{D})}X_0, \quad X_0 \in \mathbb{R}. \tag{138}$$

This implies that the dynamics of the considered interconnection is described by Σ_F once $L_3(\mathcal{D}) = \overline{L}_i(\mathcal{D})$ and $r = X_0$. Quite a similar argument applies to the other interconnections. ■

Remark 5.1. Proposition 15 makes it clear that voltage and current generators can be incorporated in the canonical representation Σ_F as feedforward blocks driven by their time integrals and whose rational function depends on either $\overline{L}_i(\mathcal{D})$ or $\overline{L}_v(\mathcal{D})$ (see Example 5.3), as reported in Table 4. Also, it follows that each one of the six interconnections admits a first integral, i.e. a scalar variable ($X(t)$ in the proof) is constant over time and its value (X_0 in the proof) is indeed the value of the input r in Σ_F.

Some illustrative examples are reported next. In particular, the third one shows how to deal with the presence of two generators.

Example 5.1. Consider again the well-known Murali–Lakshmanan–Chua oscillatory memristive circuit of Fig. 15(a) (see, e.g. [Ahamed & Lakshmanan, 2017]) where $w(t)$ is a voltage generator. It can be readily verified that $\mathbf{L}$ is described by (126) with $L_i(\mathcal{D})$ as in (10) and

$$\overline{L}_i(\mathcal{D}) = \frac{\dfrac{1}{LC}}{\mathcal{D}^2 + \dfrac{R}{L}\mathcal{D} + \dfrac{1}{LC}}. \tag{139}$$

Moreover, (130) boils down to

$$\left(\mathcal{D}^2 + \frac{R}{L}\mathcal{D} + \frac{1}{LC}\right) v_{\mathbf{L}}(t) - \left(\frac{1}{C}\mathcal{D} + \frac{R}{LC}\right) i_{\mathbf{L}}(t) = \frac{1}{LC}w(t). \tag{140}$$

Hence, Proposition 15 ensures that the circuit of Fig. 15(a) admits the canonical representation of Fig. 14 with $y = \varphi_M$, $\hat{n}(\cdot) = \hat{q}(\cdot)$ and

$$L_1(\mathcal{D}) = \frac{\dfrac{1}{C}\mathcal{D} + \dfrac{R}{LC}}{\mathcal{D}^2 + \dfrac{R}{L}\mathcal{D} + \dfrac{1}{LC}}, \quad L_2(\mathcal{D}) = \frac{1}{\mathcal{D}^2 + \dfrac{R}{L}\mathcal{D} + \dfrac{1}{LC}}, \quad L_3(\mathcal{D}) = \frac{\dfrac{1}{LC}}{\mathcal{D}^2 + \dfrac{R}{L}\mathcal{D} + \dfrac{1}{LC}}. \tag{141}$$

Example 5.2. Consider the forced circuit of Fig. 15(b) composed of the two-terminal element of Fig. 3(b), $\mathbf{MR}_q$ as **ME** and a current generator $w(t)$ in parallel to the resistor. In this case, $\mathbf{L}$ is described by (127), with $L_v(\mathcal{D})$ as in (12) and

$$\overline{L}_v(\mathcal{D}) = -\frac{\dfrac{R}{L}\mathcal{D}}{\mathcal{D}^2 + \dfrac{R}{C}\mathcal{D} + \dfrac{1}{LC}}. \tag{142}$$

The differential equation (131) reduces to

$$\left(\mathcal{D}^2 + \frac{R}{L}\mathcal{D} + \frac{1}{LC}\right) i_{\mathbf{L}}(t) - \frac{1}{L}\mathcal{D}v_{\mathbf{L}}(t) = -\frac{R}{L}\mathcal{D}w(t), \tag{143}$$

which implies that the circuit of Fig. 15(b) admits the canonical representation of Fig. 14 with $y = q_M$,

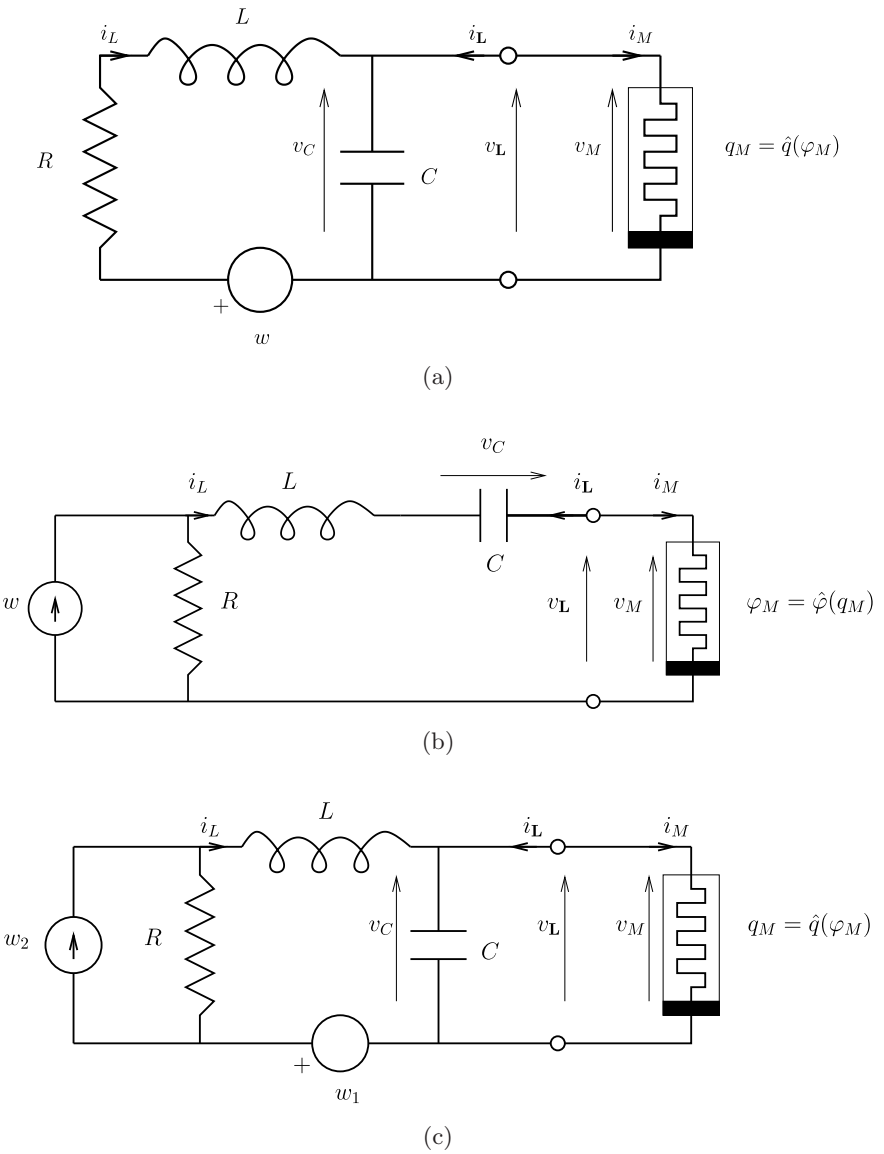

Fig. 15. Nonautonomous circuits: (a) Example 5.1, (b) Example 5.2 and (c) Example 5.3.

$\hat{n}(\cdot) = \hat{\varphi}(\cdot)$ and

$$L_1(\mathcal{D}) = \frac{\frac{1}{L}\mathcal{D}}{\mathcal{D}^2 + \frac{R}{C}\mathcal{D} + \frac{1}{LC}},$$
$$L_2(\mathcal{D}) = \frac{1}{\mathcal{D}^2 + \frac{R}{C}\mathcal{D} + \frac{1}{LC}}, \tag{144}$$
$$L_3(\mathcal{D}) = -\frac{\frac{R}{L}\mathcal{D}}{\mathcal{D}^2 + \frac{R}{C}\mathcal{D} + \frac{1}{LC}}.$$

Example 5.3. Consider the circuit of Fig. 15(c) which has the same structure as that of Example 5.1 with an additional current generator. In this case the current–voltage model of $\mathbf{L}$ is described by the following input–output relation

$$v_{\mathbf{L}}(t) = L_i(\mathcal{D})i_{\mathbf{L}}(t) + \overline{L}_{i1}(\mathcal{D})w_1(t) + \overline{L}_{i2}(\mathcal{D})w_2(t), \tag{145}$$

where $L_i(\mathcal{D})$ is given in (10), while $\overline{L}_{i1}(\mathcal{D}) = \overline{L}_i(\mathcal{D})$ and $\overline{L}_{i2}(\mathcal{D}) = R\overline{L}_i(\mathcal{D})$ with $\overline{L}_i(\mathcal{D})$ as in (139). The corresponding differential equation is

$$\left(\mathcal{D}^2 + \frac{R}{L}\mathcal{D} + \frac{1}{LC}\right) v_{\mathbf{L}}(t) - \left(\frac{1}{C}\mathcal{D} + \frac{R}{LC}\right) i_{\mathbf{L}}(t) = \frac{1}{LC}w_1(t) + \frac{R}{LC}w_2(t). \tag{146}$$

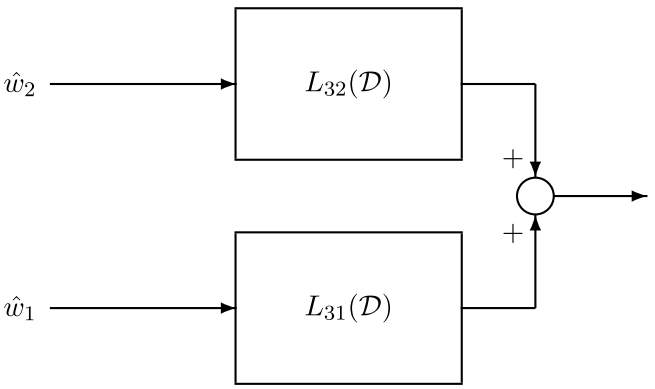

Fig. 16. Example 5.3: block representation of the feedforward system which replaces that driven by $\hat{w}$ in Fig. 14.

Hence, according to Remark 5.1, the circuit of Fig. 15(c) admits the canonical representation of Fig. 14, once the feedforward subsystem driven by $\hat{w}$ is substituted by the system of Fig. 16 given by the parallel interconnection of two linear subsystems driven by the input signals $\hat{w}_1$ and $\hat{w}_2$, which are defined according to (132). Specifically, we have $y = \varphi_M$, $\hat{n}(\cdot) = \hat{q}(\cdot)$, $L_1(\mathcal{D})$ and $L_2(\mathcal{D})$ as in (141), $L_{31}(\mathcal{D}) = L_3(\mathcal{D})$ and $L_{32}(\mathcal{D}) = RL_3(\mathcal{D})$ with $L_3(\mathcal{D})$ as in (141).

6. Conclusions

A novel input–output approach to investigate the dynamical properties of a class of circuits with memelements has been proposed. The circuits are given by the interconnection of a linear time-invariant two-terminal (one-port) element and an ideal memelement. The two-terminal element can be either passive or active, while the memelement can be a (flux- or charge-controlled) memristor, a (flux- or σ-controlled) memcapacitor or a (charge- or ρ-controlled) meminductor.

It is first shown that the dynamics of any circuit of the class admits a first integral, thus implying that the circuit can be represented via a reduced-order input–output system. In particular, the two-port element must be active in the case of a flux-controlled memcapacitor and a charge-controlled meminductor, while it can be also passive in all the other cases. Interestingly, the reduced-order system enjoys a structure which is quite popular in the area of control systems, i.e. it is composed of an internal feedback interconnection between a linear dynamical subsystem and a nonlinear memoryless one, plus a feedforward linear dynamical system driven by an external constant input. Moreover, it turns out that the dynamics of the reduced-order system is exactly the same as that displayed by a circuit with a standard nonlinear resistor/capacitor/inductor in place of the memristor/memcapacitor/meminductor and an additional constant generator. It is also shown that the existence of the first integral, and hence of the reduced-order system, implies the presence of invariant manifolds in the state space representation of the circuit. An explicit expression of the invariant manifolds in the voltage–current state space is developed for any circuit, also pointing out cases where the invariant manifolds are linear. Finally, it is shown how the case of circuits forced by external generators can be readily encompassed within the proposed approach. Several examples are considered throughout the paper for illustrative purposes.

Future research issues are the extension of the developed input–output approach to circuits containing more than one memelement and the exploitation of the structure of the reduced-order system for tackling analysis and control problems in the emerging area of multistability control.

References

Adamatzky, A. & Chua, L. (eds.) [2014] *Memristor Networks* (Springer, NY).

Ahamed, A. & Lakshmanan, M. [2017] "Discontinuity induced Hopf and Neimark–Sacker bifurcations in a memristive Murali–Lakshmanan–Chua circuit," *Int. J. Bifurcation and Chaos* **27**, 1730021-1–21.

Amador, A., Freire, E., Ponce, E. & Ros, J. [2017] "On discontinuous piecewise linear models for memristor oscillators," *Int. J. Bifurcation and Chaos* **27**, 1730022-1–18.

Appeltant, L., Soriano, M., Van der Sande, G., Danckaert, J., Massar, S., Dambre, J., Schrauwen, B., Mirasso, C. & Fischer, I. [2011] "Information processing using a single dynamical node as complex system," *Nat. Commun.* **2**, 468.

Atherton, D. P. [1975] *Nonlinear Control Engineering* (Van Nostrand Reinhold, London).

Bao, B., Jiang, T., Xu, Q., Chen, M., Wu, H. & Hu, Y. [2016] "Coexisting infinitely many attractors in active band-pass filter-based memristive circuit," *Nonlin. Dyn.* **86**, 1711–1723.

Basso, M., Genesio, R. & Tesi, A. [1997] "A frequency method or predicting limit cycle bifurcations," *Nonlin. Dyn.* **13**, 339–360.

Biolek, D., Biolek, Z. & Biolkova, V. [2011] "Pinched hysteretic loops of ideal memristors, memcapacitors and meminductors must be 'self-crossing'," *Electron. Lett.* **47**, 1385–1387.

Biolek, D., Di Ventra, M. & Pershin, Y. V. [2013] "Reliable spice simulations of memristors, memcapacitors and meminductors," *Radioengineering* **22**, 945.

Bonani, F. & Gilli, M. [1999] "Analysis of stability and bifurcations of limit cycles in Chua's circuit through the harmonic-balance approach," *IEEE Trans. Circuits Syst.-I* **46**, 881–890.

Chang, H., Li, Y., Yuan, F. & Chen, G. [2019] "Extreme multistability with hidden attractors in a simplest memristor-based circuit," *Int. J. Bifurcation and Chaos* **29**, 1950086-1–17.

Chen, M., Sun, M., Bao, B., Wu, H., Xu, Q. & Wang, J. [2018] "Controlling extreme multistability of memristor emulator-based dynamical circuit in flux-charge domain," *Nonlin. Dyn.* **91**, 1395–1412.

Chen, M., Sun, M., Bao, H., Hu, Y. & Bao, B. [2020] "Flux-charge analysis of two-memristor-based Chua's circuit: Dimensionality decreasing model for detecting extreme multistability," *IEEE Trans. Indust. Electron.* **67**, 2197–2206.

Chua, L. [1971] "Memristor-the missing circuit element," *IEEE Trans. Circuit Th.* **18**, 507–519.

Chua, L. [1980] "Device modeling via nonlinear circuit elements," *IEEE Trans. Circuits Syst.* **27**, 1014–1044.

Chua, L. [2009 (reaffirmed 2013)] "Introduction to memristors," IEEE Digital Library: https://ieeexplore.ieee.org/courses/details/EDP091.

Chua, L. [2015] "Everything you wish to know about memristors but are afraid to ask," *Radioengineering* **24**, 319–368.

Corinto, F. & Forti, M. [2016] "Memristor circuits: Flux-charge analysis method," *IEEE Trans. Circuits Syst.-I*: *Reg. Papers* **63**, 1997–2009.

Corinto, F. & Forti, M. [2017] "Memristor circuits: Bifurcations without parameters," *IEEE Trans. Circuits Syst.-I*: *Reg. Papers* **64**, 1540–1551.

Corinto, F. & Forti, M. [2018] "Memristor circuits: Pulse programming via invariant manifolds," *IEEE Trans. Circuits Syst.-I*: *Reg. Papers* **65**, 1327–1339.

Corinto, F., Di Marco, M., Forti, M. & Chua, L. [2019] "Nonlinear networks with mem-elements: Complex dynamics via flux-charge analysis method," *IEEE Trans. Cybern.* **Early Access**, 1–14, doi:10.1109/TCYB.2019.2904903.

Di Marco, M., Forti, M. & Tesi, A. [2003] "Harmonic balance approach to predict period-doubling bifurcations in nearly-symmetric neural networks," *J. Circuits Syst. Comput.* **12**, 435–460.

Di Marco, M., Forti, M., Innocenti, G. & Tesi, A. [2018] "Harmonic balance method to analyze bifurcations in memristor oscillatory circuits," *Int. J. Circuit Th. Appl.* **46**, 66–83.

Di Marco, M., Innocenti, G., Forti, M. & Tesi, A. [2019] "Control design for targeting dynamics of memristor Murali–Lakshmanan–Chua circuit," *18th European Control Conf.* (*ECC2019*), pp. 4332–4337.

Di Ventra, M., Pershin, Y. & Chua, L. [2009] "Circuit elements with memory: Memristors, memcapacitors, and meminductors," *Proc. IEEE* **97**, 1717–1724.

Fiedler, B., Liebscher, S. & Alexander, J. [2000] "Generic Hopf bifurcation from lines of equilibria without parameters: I. Theory," *J. Diff. Eqs.* **167**, 16–35.

Genesio, R. & Tesi, A. [1992] "Harmonic balance methods for the analysis of chaotic dynamics in nonlinear systems," *Automatica* **28**, 531–548.

Georgiou, J., Kossifos, K., Antoniades, M., Jaafar, A. & Kemp, N. [2018] "Chua mem-components for adaptive RF metamaterials," *IEEE Int. Symp. Circuits and Systems* (*ISCAS2018*) (IEEE), pp. 1–5.

Innocenti, G., Tesi, A. & Genesio, R. [2010] "Complex behaviour analysis in quadratic jerk systems via frequency domain Hopf bifurcation," *Int. J. Bifurcation and Chaos* **20**, 657–667.

Innocenti, G., Di Marco, M., Forti, M. & Tesi, A. [2019a] "A controlled Murali–Lakshmanan–Chua memristor circuit to mimic neuron dynamics," *58th IEEE Conf. Decision and Control* (*CDC19*) (IEEE).

Innocenti, G., Di Marco, M., Forti, M. & Tesi, A. [2019b] "Prediction of period doubling bifurcations in harmonically forced memristor circuits," *Nonlin. Dyn.* **96**, 1169–1190.

Jensen, J. & Tufte, G. [2017] "Reservoir computing with a chaotic circuit," *European Conf. Artificial Life 14* (MIT Press), pp. 222–229.

Khalil, H. K. [2002] *Nonlinear Systems*, 3rd edition (Prentice-Hall, Upple Saddle River, NJ).

Li, C., Li, C., Huang, T. & Wang, H. [2013] "Synaptic memcapacitor bridge synapses," *Neurocomputing* **122**, 370–374.

Li, Q., Hu, S., Tang, S. & Zeng, G. [2014] "Hyperchaos and horseshoe in a 4D memristive system with a line of equilibria and its implementation," *Int. J. Circuit Th. Appl.* **42**, 1172–1188.

Li, C., Wang, Z., Rao, M., Belkin, D., Song, W., Jiang, H., Yan, P., Li, Y., Lin, P., Hu, M. *et al.* [2019] "Long short-term memory networks in memristor crossbar arrays," *Nat. Mach. Intell.* **1**, 49.

Mazumder, P., Kang, S. M. & Waser, R. (eds.) [2012] "Special issue on memristors: Devices, models, and applications," *Proc. IEEE* **100**, 1911-1919.

Mees, A. I. [1981] *Dynamics of Feedback Systems* (Wiley, NY).

Messias, M., Nespoli, C. & Botta, V. [2010] "Hopf bifurcation from lines of equilibria without parameters in memristor oscillators," *Int. J. Bifurcation and Chaos* **20**, 437–450.

Pei, J.-S., Wright, J. P., Todd, M. D., Masri, S. F. & Gay-Balmaz, F. [2015] "Understanding memristors and memcapacitors in engineering mechanics applications," *Nonlin. Dyn.* **80**, 457–489.

Pérez-Tomás, A. [2019] "Functional oxides for photoneuromorphic engineering: Toward a solar brain," *Advanced Materials Interfaces* **6**, 1900471.

Pershin, Y. & Di Ventra, M. [2011] "Memory effects in complex materials and nanoscale systems," *Adv. Phys.* **60**, 145–227.

Piccardi, C. [1994] "Bifurcations of limit cycles in periodically forced nonlinear systems: The harmonic balance approach," *IEEE Trans. Circuits Syst.-I* **41**, 315–320.

Pisarchik, A. & Feudel, U. [2014] "Control of multistability," *Phys. Rep.* **540**, 167–218.

Ponce, E., Ros, J., Freire, E. & Amador, A. [2017] "Unravelling the dynamical richness of 3D canonical memristor oscillators," *Microelectron. Eng.* **182**, 15–24.

Radwan, A. G. & Fouda, M. E. [2015] *On the Mathematical Modeling of Memristor, Memcapacitor, and Meminductor*, Vol. 26 (Springer).

Rajagopal, K., Jafari, S., Karthikeyan, A., Srinivasan, A. & Ayele, B. [2018] "Hyperchaotic memcapacitor oscillator with infinite equilibria and coexisting attractors," *Circuits Syst. Sign. Process.* **37**, 3702–3724.

Scarabello, M. & Messias, M. [2014] "Bifurcations leading to nonlinear oscillations in a 3D piecewise linear memristor oscillator," *Int. J. Bifurcation and Chaos* **24**, 1430001-1–18.

Strukov, D. B., Snider, G. S., Stewart, D. R. & Williams, R. S. [2008] "The missing memristor found," *Nature* **453**, 80.

Tesi, A., Abed, E. H., Genesio, R. & Wang, H. O. [1996] "Harmonic balance analysis of period-doubling bifurcations with implications for control of nonlinear dynamics," *Automatica* **32**, 1255–1271.

Tetzlaff, R. (ed.) [2014] *Memristors and Memristive Systems* (Springer, NY).

Traversa, F. & Di Ventra, M. [2015] "Universal memcomputing machines," *IEEE Trans. Neural Netw. Learn. Syst.* **26**, 2702–2715.

Varshney, V., Sabarathinam, S., Prasad, A. & Thamilmaran, K. [2018] "Infinite number of hidden attractors in memristor-based autonomous Duffing oscillator," *Int. J. Bifurcation and Chaos* **28**, 1850013-1–13.

Waldrop, M. M. [2016] "The chips are down for Moore's law," *Nature News* **530**, 144.

Wang, X., Yu, J., Jin, C., Iu, H. H. C. & Yu, S. [2019] "Chaotic oscillator based on memcapacitor and meminductor," *Nonlin. Dyn.* **96**, 161–173.

Williams, R. S. [2017] "What's next? [The end of Moore's law]," *Comput. Sci. Engin.* **19**, 7–13.

Xu, B., Wang, G. & Shen, Y. [2017] "A simple meminductor-based chaotic system with complicated dynamics," *Nonlin. Dyn.* **88**, 2071–2089.

Yuan, F., Wang, G., Jin, P., Wang, X. & Ma, G. [2016a] "Chaos in a meminductor-based circuit," *Int. J. Bifurcation and Chaos* **26**, 1650130-1–14.

Yuan, F., Wang, G., Shen, Y. & Wang, X. [2016b] "Coexisting attractors in a memcapacitor-based chaotic oscillator," *Nonlin. Dyn.* **86**, 37–50.

Yuan, F., Li, Y., Wang, G., Dou, G. & Chen, G. [2019] "Complex dynamics in a memcapacitor-based circuit," *Entropy* **21**, 188.

Zhang, Y., Guo, M., Dou, G., Li, Y. & Chen, G. [2019] "Oscillatory circuits built on physical SBT memristor," *Int. J. Bifurcation and Chaos* **29**, 1950097-1–21.

Zidan, M. A., Strachan, J. P. & Lu, W. D. [2018] "The future of electronics based on memristive systems," *Nat. Electron.* **1**, 22.

Appendix

Proof of Proposition 10. We first need the following preliminary result.

Lemma A.1. *Consider the nonlinear state transformation* $T^{(I)} : \mathbb{R}^{N+1} \to \mathbb{R}^{N+1}$ *from* $(\xi_1, x)^\top \in \mathbb{R}^{N+1}$ *to* $\eta \in \mathbb{R}^{N+1}$ *defined as*

$$T^{(I)}: \begin{cases} \eta_1 = \xi_1, \\ \eta_i = x_{i-1} + p_{N+1-i}\xi_1 + r_{N+1-i} f(\xi_1), \\ \qquad\qquad i = 2, \ldots, N+1. \end{cases} \tag{A.1}$$

Then, $T^{(I)}$ *is invertible on* $\mathbb{R}^{N+1}$ *and* $\mathcal{S}^{(I)}$ *admits the following equivalent representation*

$$\mathcal{S}^{(I)}_{\text{eq}}: \begin{cases} \begin{pmatrix} \mathcal{D}\eta_1(t) \\ \mathcal{D}\eta_2(t) \\ \vdots \\ \mathcal{D}\eta_{N-1}(t) \\ \mathcal{D}\eta_N(t) \end{pmatrix} = A \begin{pmatrix} \eta_1(t) \\ \eta_2(t) \\ \vdots \\ \eta_{N-1}(t) \\ \eta_N(t) \end{pmatrix} - Bf(\eta_1(t)) + \begin{pmatrix} 0 \\ 0 \\ \vdots \\ 0 \\ \eta_{N+1}(t) \end{pmatrix}, \\ \mathcal{D}\eta_{N+1}(t) = 0. \end{cases} \tag{A.2}$$

Proof. Observe that the $N+1$ equations of $\mathcal{S}^{(I)}$ in (103) can be rearranged as

$$\begin{cases} \mathcal{D}\xi_1(t) = x_1(t) \\ \mathcal{D}x_1(t) + p_{N-1}x_1(t) + r_{N-1}f'(\xi_1(t))x_1(t) = x_2(t) \\ \qquad\qquad \vdots \\ \mathcal{D}x_{N-2}(t) + p_2x_1(t) + r_2f'(\xi_1(t))x_1(t) = x_{N-1}(t) \\ \mathcal{D}x_{N-1}(t) + p_1x_1(t) + r_1f'(\xi_1(t))x_1(t) = x_N(t) \\ \mathcal{D}x_{N+1}(t) + p_0x_1(t) + r_0f'(\xi_1(t))x_1(t) = 0. \end{cases} \tag{A.3}$$

By taking into account that

$$f'(\xi(t))x_1(t) = f'(\xi(t))\mathcal{D}\xi(t) = \mathcal{D}f(\xi(t))$$

and exploiting (A.1), (A.3) can be equivalently rewritten as

$$\begin{cases} \mathcal{D}\eta_1(t) = x_1(t) \\ \mathcal{D}\eta_2(t) = x_2(t) \\ \qquad\qquad \vdots \\ \mathcal{D}\eta_{N-1}(t) = x_{N-1}(t) \\ \mathcal{D}\eta_N(t) = x_N(t) \\ \mathcal{D}\eta_{N+1}(t) = 0. \end{cases} \tag{A.4}$$

By inverting the nonlinear transformation $T^{(I)}$ we can obtain $x_1, \ldots, x_N$ in terms of $\eta_1, \ldots, \eta_{N+1}$ and rewrite (A.4) as

$$\begin{cases} \mathcal{D}\eta_1(t) = -p_{N-1}\eta_1(t) + \eta_2(t) - r_{N-1}f(\eta_1(t)) \\ \mathcal{D}\eta_2(t) = -p_{N-2}\eta_1(t) + \eta_3(t) - r_{N-2}f(\eta_1(t)) \\ \qquad\qquad \vdots \\ \mathcal{D}\eta_{N-1}(t) = -p_1\eta_1(t) + \eta_N(t) - r_1f(\eta_1(t)) \\ \mathcal{D}\eta_N(t) = -p_0\eta_1(t) + \eta_{N+1}(t) - r_0f(\eta_1(t)) \\ \mathcal{D}\eta_{N+1}(t) = 0, \end{cases} \tag{A.5}$$

thus completing the proof. ■

Now, from the last equation of (A.2) it follows that each solution $\eta(t) \in \mathbb{R}^{N+1}$ of $\mathcal{S}^{(I)}_{\text{eq}}$ is such that:

$$\eta_{N+1}(t) = \eta_{N+1}(t_0), \quad \forall\, t \geq t_0. \tag{A.6}$$

This implies that the hyperplane $\eta_{N+1} = K_0^{(I)}$, with $K_0^{(I)} = \eta_{N+1}(t_0)$, is an invariant manifold of $\mathcal{S}^{(I)}_{\text{eq}}$. Now, the last equation of (A.1) ensures that

$$x_N + p_0\xi_1 + r_0f(\xi_1) = K_0^{(I)}$$

is indeed an invariant manifold of $\mathcal{S}^{(I)}$. Hence, it follows the solution $(\xi(t), x(t))^\top$ with initial condition $(\xi(t_0), x(t_0))^\top$ is such that

$$\begin{aligned} &x_N(t) + p_0\xi_1(t) + r_0f(\xi_1(t)) \\ &\quad = x_N(t_0) + p_0\xi_1(t_0) + r_0f(\xi_1(t_0)), \quad \forall\, t \geq t_0, \end{aligned} \tag{A.7}$$

thus proving (104).

To complete the proof we observe that the dynamics on the invariant manifold $\mathcal{M}_0^{(I)}$ can be obtained by first determining the dynamics on the invariant hyperplane $\eta_{N+1} = K_0^{(I)}$ in terms of $\eta_1(t), \ldots, \eta_N(t)$ and then by inverting the nonlinear transformation $T^{(I)}$ to get $\xi_1(t), x_1(t), \ldots, x_N(t)$. Indeed, the dynamics of the invariant hyperplane is described by $\mathcal{S}_R^{(I)}$ since its equations are exactly equal to the first N equations of (A.5) once $\eta_{N+1} = K_0^{(I)}$. Also, Eqs. (106) are exactly those obtained by solving (A.1) with respect to $\xi_1, x_1, \ldots, x_N$ with $\eta_{N+1} = K_0^{(I)}$, thus completing the proof. ■

Proof of Proposition 12. The proof is based on the following preliminary result.

Lemma A.2. *Consider the nonlinear state transformation $T^{(II)} : \mathbb{R}^{N+1} \to \mathbb{R}^{N+1}$ from $(\xi_1, x)^\top \in \mathbb{R}^{N+1}$ to $\eta \in \mathbb{R}^{N+1}$ defined as*

$$T^{(II)}: \begin{cases} \eta_1 = \xi_1, \\ \eta_2 = x_1 + p_{N-1}\xi_1 + r_{N-2}f(\xi_1), \\ \eta_i = x_{i-1} + p_{N+1-i}\xi_1 + r_{N-i}f(\eta_1) \\ \qquad + r_{N+1-i}f'(\xi_1)x_1, \quad i = 3, \ldots, N, \\ \eta_{N+1} = x_N + p_0\xi_1 + r_0f'(\xi_1(t))x_1. \end{cases} \tag{A.8}$$

Then, $T^{(II)}$ is invertible on $\mathbb{R}^{N+1}$ and $\mathcal{S}^{(II)}$ admits the following equivalent representation

$$\mathcal{S}^{(II)}_{\text{eq}}: \begin{cases} \begin{pmatrix} \mathcal{D}\eta_1(t) \\ \mathcal{D}\eta_2(t) \\ \vdots \\ \mathcal{D}\eta_{N-1}(t) \\ \mathcal{D}\eta_N(t) \end{pmatrix} = A \begin{pmatrix} \eta_1(t) \\ \eta_2(t) \\ \vdots \\ \eta_{N-1}(t) \\ \eta_N(t) \end{pmatrix} - B_0 f(\eta_1(t)) + \begin{pmatrix} 0 \\ 0 \\ \vdots \\ 0 \\ \eta_{N+1}(t) \end{pmatrix}, \\ \mathcal{D}\eta_{N+1}(t) = 0. \end{cases} \tag{A.9}$$

Proof. The proof parallels that of Lemma A.1 once $T^{(I)}$ is replaced by $T^{(II)}$. ■

Given Lemma A.2, the proof Proposition 12 follows by reasoning as in Proposition 10. ■

Proof of Proposition 14. The proof is based on the following preliminary result.

Lemma A.3. *Consider the nonlinear state transformation $T^{(III)}: \mathbb{R}^{N+2} \to \mathbb{R}^{N+2}$ from $(\xi_1, \xi_2, x)^\top \in \mathbb{R}^{N+2}$ to $\eta \in \mathbb{R}^{N+2}$ defined as*

$$\begin{cases} \eta_1 = \xi_1, \\ \eta_2 = p_{N-1}\xi_1 + \xi_2 + r_N f(\xi_1), \\ \eta_i = x_{i-2} + p_{N+1-i}\xi_1 + p_{N+2-i}\xi_2 \\ \qquad + r_{N+2-i} f(\xi_1), \quad i = 3, \ldots, N+1, \\ \eta_{N+2} = x_N + p_0\xi_2 + r_0 f(\xi_1). \end{cases} \tag{A.10}$$

Then, $T^{(III)}$ is invertible on $\mathbb{R}^{N+2}$ and $\mathcal{S}^{(III)}$ admits the following equivalent representation

$$\mathcal{S}^{(III)}_{\text{eq}}: \begin{cases} \begin{pmatrix} \mathcal{D}\eta_1(t) \\ \mathcal{D}\eta_2(t) \\ \vdots \\ \mathcal{D}\eta_N(t) \\ \mathcal{D}\eta_{N+1}(t) \end{pmatrix} = \begin{pmatrix} A & 0_{1\times N} \\ 0_{N\times 1} & 0 \end{pmatrix} \begin{pmatrix} \eta_1(t) \\ \eta_2(t) \\ \vdots \\ \eta_N(t) \\ \eta_{N+1}(t) \end{pmatrix} - \begin{pmatrix} D \\ B \end{pmatrix} f(\eta_1(t)) + \begin{pmatrix} 0 \\ 0 \\ \vdots \\ 0 \\ \eta_{N+2}(t) \end{pmatrix}, \\ \mathcal{D}\eta_{N+2}(t) = 0. \end{cases} \tag{A.11}$$

Proof. The proof parallels that of Lemma A.1 once $T^{(I)}$ is replaced by $T^{(III)}$. ■

Given Lemma A.3, the proof is completed via an argument similar to that used in Proposition 10. ■